Stress-Strain Behavior of Ottawa Sand in Cyclic Direct Simple Shear and Modeling of Cyclic Strength using Artificial Neural Networks

2 3 4

1

Sarra Lbibb¹, Majid T. Manzari²

5

8

6 Department of Civil and Environmental Engineering, George Washington University, 7 Washington, DC, USA

ABSTRACT

- 9 The stress-strain behavior of Ottawa F65 sand is investigated through an extensive series of 10 constant volume stress-controlled cyclic direct simple shear (CDSS) tests performed at different 11 densities, overburden pressures, and static shear stresses prior to cyclic shearing to quantify their effects on the cyclic strength of Ottawa F65 sand. Results of the CDSS tests are used in the 12 constitutive model calibration exercise for the Liquefaction Experiments and Analysis Project 13 14 (LEAP-2022). The collected database of CDSS tests is used to develop an Artificial Neural 15 Networks (ANN) model capable of predicting Ottawa F65 liquefaction strength for a specified set of relative density, overburden pressure, static shear stress ratio, and cyclic shear stress ratio. After 16 17 training, validation and testing, the ANN model is further assessed using blind prediction of the 18 liquefaction strength in new CDSS tests for a relative density and overburden stress that are not 19 available in the training dataset. CDSS tests under similar conditions were then carried out in the 20 laboratory for validation of the ANN model. The comparisons of the predictions with the 21 experimental results have demonstrated the ANN model predictive capability for liquefaction 22 strength and its sensitivity to changes in relative density, overburden stress and cyclic stress ratio.
- 23 Keywords
- 24 Cyclic direct simple shear tests (CDSS), Liquefaction strength, Ottawa F65 sand, Artificial Neural
- 25 Network.

26 1. Introduction

- 27 Soil liquefaction has been observed to cause excessive ground displacement including lateral
- spreading and settlement, and extensive damage to structures [1]. The phenomenon is generally
- 29 observed in loose to medium dense saturated granular soils that develop significant excess pore
- 30 pressure under cyclic shearing in undrained condition. Many aspects of the stress-strain response
- 31 of liquefiable soils have been studied extensively in the past few decades and a large number of
- 32 empirical relationships have been developed for estimation of liquefaction strength of sandy soils.
- 33 The main focus of the current work is to extend the extensive dataset available on the stress-strain-

¹ Corresponding author. slbibb58@gwu.edu

² manzari@gwu.edu

Postal address: Department of Civil and Environmental Engineering, The George Washington University, 800 22nd St. NW, Washington, DC 20052, USA.

- 34 strength response of Ottawa F65 sand and to facilitate the use of the extended dataset for calibration
- 35 of advanced constitutive models and machine learning techniques.
- 36 In this study, the cyclic stress-strain behavior and liquefaction strength of Ottawa F65 sand are
- 37 investigated through multiple series of stress-controlled constant volume cyclic direct simple shear
- 38 (CDSS) tests. The experimental campaign aimed to study the effects of soil density, overburden
- 39 stress, and static shear stress on the liquefaction strength. The collected database of CDSS tests is
- 40 used to develop an Artificial Neural Networks (ANN) model with the objective of predicting the
- 41 cyclic strength of Ottawa F65 sand for densities and loading conditions that are not covered in the
- 42 experiments.
- 43 The CDSS tests were performed in dry conditions where a constant volume condition is enforced
- 44 by constraining the vertical and lateral displacements of the soil specimen. Soil contraction results
- in decreased vertical effective stress and soil dilation results in increased vertical effective stress 45
- 46 to maintain a constant volume condition, which is respectively equivalent to increased excess pore
- 47 water pressure (soil contraction) and decreased excess pore water pressure (soil dilation) in
- 48 undrained condition. Therefore, the variation of vertical effective stress in constant volume
- 49 condition is related to the variation of excess pore water pressure in undrained condition [2].
- 50 Constant volume direct simple shear tests have been widely used to investigate liquefaction of
- 51 sands. For instance, Wijewickreme et al. [3] have investigated the cyclic response of loose Fraser
- 52 River sand using constant volume CDSS tests conducted on air-pluviated and water-pluviated
- 53 specimens. In addition to considering the effects of confining stress and initial static shear stress,
- the study has also demonstrated the importance of soil fabric on the cyclic resistance of sands. Da 54
- 55 Fonseca et al. [4] have also used constant volume CDSS tests conducted on two different types of
- 56 sandy soils to evaluate the correction factor related to the magnitude of confining stress.
- 57 The stress-strain behavior of sands under monotonic and cyclic loading conditions has been
- 58 extensively investigated in the literature using laboratory element tests (triaxial tests, direct simple
- 59 shear tests, torsional simple shear tests). This has emerged with the work of Seed and Lee [5]
- 60 where the factors affecting sand liquefaction were studied through undrained triaxial tests on
- 61 isotropically consolidated saturated sand specimens. Among the available testing options, the
- direct simple shear test has attracted significant interest in practice because of the relative ease in 62
- 63 the specimen preparation and the ability to conduct constant volume tests without saturating the
- 64 soil. Several recent studies have investigated the stress-strain response of sandy soils in direct
- 65 simple shear tests by exploring the factors affecting the soil response and examining some
- 66 limitations of the direct simple shear testing option. Wai et al. [6] have investigated the effect of imperfection in boundary conditions on the results of monotonic and cyclic direct simple shear 67
- 68 tests. The near-frictionless vertical boundaries result in a non-uniform stress distribution near the
- boundaries. Also, vertical compliance can result in high axial strain that may alter the constant 69
- 70 volume condition. It was concluded that while near-frictionless vertical boundaries in the DSS test
- 71 can be used to approximate simple shear conditions, and the effect of top-cap tilting is negligible,
- 72 vertical compliance can significantly affect the measured response of sandy soils.
- 73 Several past studies have demonstrated the multi-parameter dependence of soil response. Castro
- 74 and Poulos [7] and Ishihara [8] have demonstrated that cyclic resistance increases with increased

soil density and decreased initial confining stress. Idriss and Boulanger [9] have developed a correction factor to account for the effect of overburden stress on liquefaction strength of sandy soils. In the case of a sloping ground, the consideration of a static shear stress prior to cyclic shearing was shown to impact the liquefaction strength [10-12]. Seed [10] has introduced a correction factor to account for the effect of static shear stress ratio on the liquefaction strength of sandy soils. The correction factors to account for the effects of overburden stress and static shear stress ratio were shown to be dependent on soil relative density that is also correlated with normalized SPT N-values and CPT tip resistance [9,11]. Park et al. [12] have conducted a series of cyclic direct simple shear tests on loose and dense Nakdong River sand specimens. The study showed that increased vertical effective stress results in decreased cyclic strength. The decrease of cyclic resistance with increased vertical effective stress is more significant in cases where initial static shear stresses are considered. The increase of static shear stress ratio was shown to decrease the cyclic strength for looser specimens. The effect of static shear stress on cyclic strength of denser specimen were observed to depend on the applied vertical effective stress. It was also shown that the increase of cyclic strength with higher relative densities is more significant for cases with higher initial static shear stress levels. Park et al. [12] have measured the correction factor to account for the effect of static shear stress in a series of CDSS tests on Nakdong River sand. The correction factor to account for this effect is measured as the ratio of cyclic resistance ratio at a non-zero static shear stress ratio α to cyclic resistance ratio at a static shear stress ratio of zero $(CRR_{\alpha}/CRR_{\alpha=0})$. These ratios were obtained for a moment magnitude of earthquake M=7.5, which corresponds to cyclic strength at 15 uniform stress cycles [13]. It was concluded that the increase in static shear stress ratio results in a decreased correction factor for loose specimens, which indicates that cyclic strength has decreased with higher static shear stress. For denser specimens, the correction factor was observed to increase with increased static shear stress ratio for a vertical effective stress of 100 kPa. However, for moderate and higher vertical effective stresses (150 kPa and 200 kPa), the variation of the measured correction factor with static shear stress ratio shows first an increase followed by a decreasing trend. The results of the experiments presented by Park et al. [12] showed that for dense specimens, the experimentally measured correction factors K_{α} are overestimated by the correlations proposed by Idriss and Boulanger [9].

75

76

77

78

79

80

81

8283

84

85

8687

88

89 90

91

92

93

94

95 96

97

98

99

100

101102

103

104

105

106

107

108109

110111

112

113

114

115

116

Loading frequency may also influence the liquefaction strength. By considering various loading frequencies while performing element tests, some studies have reported that the cyclic strength is uninfluenced or slightly influenced by the loading frequency by conducting cyclic simple shear tests on Monterey sand under a vertical confining stress of 500 kPa and a relative density of 50% [14], cyclic torsional tests on Bandaijima sand under a vertical confining stress of 33 kPa and a relative density of 37% [15], cyclic triaxial tests on Monterey sand under a vertical confining stress of 100 kPa and a relative density of 60% [16], and cyclic triaxial tests on Toyoura sand under a vertical confining stress of 100 kPa and a relative density of 50% [17]. Other studies have found that the loading frequency significantly increases the liquefaction resistance by conducting cyclic triaxial tests on EI Monte sand and Silt under a vertical confining stress of 100 kPa and relative densities of 50% and 75% [18], cyclic triaxial tests on Fujian sand under a vertical confining stress of 100 kPa and a relative density of 30% [19], and cyclic triaxial tests on a sandy soil subjected to vertical stresses of 100 kPa to 300 kPa and prepared at relative densities of 28% to 70%. Therefore,

it can be concluded that loading frequency may increase the liquefaction strength or leave it unchanged. In this study, all CDSS tests were conducted under similar loading frequency to eliminate eventual effects of loading frequency on the obtained liquefaction strength.

120 Cappellaro et al. [21] have conducted cyclic undrained direct simple shear tests on Christchurch 121 sandy soil specimens prepared by water sedimentation to replicate the fabric of fluvial soil 122 deposits. The study has considered two sands, a non-plastic silt, and their mixtures. The combined effect of soil density and fines content on liquefaction strength was investigated by preparing 123 124 specimens at two relative densities and different fines contents. The study has demonstrated 125 differences in the sensitivity of liquefaction strength to changes in soil relative density and fines 126 content between the two sands. It was concluded that liquefaction strength may decrease or remain 127 constant with increased fines content and the effect of fines content on liquefaction strength is 128 dependent on particle size distribution of the soil-fines mixture. The different soil fractions 129 considered in soil mixtures have resulted in different soil fabrics, which has led to different 130 relationships between liquefaction resistance, relative density, and fines content. The difference in 131 soil fabric affected the density state, the role of fines, and the resulting soil behavior under 132 shearing. In monotonic DSS tests, the study showed that soil fabric does not influence the position 133 of the critical state line of the studied sandy soil.

134

135

136137

138

139

140

141

142143

144

145

146

147148

149

150

151

152

153

154

155

156157

The CDSS tests conducted in the present study intend to further characterize the cyclic response of Ottawa F65 sand and complement the existing database on Ottawa F65 sand developed as part of the Liquefaction Experiments and Analysis Project LEAP [22-24]. The CDSS tests were conducted on samples prepared using constant height dry pluviation method used in the LEAP-GWU-2015 [25], LEAP-UCD-2017 [26], and LEAP-Asia-2019 [27]. Since the CDSS tests were stress-controlled and conducted on relatively dense specimens, the soil was expected to experience cyclic mobility. The liquefaction strength is quantified as the number of cycles required for the soil to reach a specific magnitude of shear strain amplitude. The shear strain amplitude can range from 2% single amplitude to 10% double amplitude shear strain [28]. Previous studies have conducted a thorough characterization of Ottawa F65 sand by determining the soil specific gravity, particle size distribution, hydraulic conductivity, and maximum and minimum void ratios [29-32]. Moreover, the soil stress-strain strength response was extensively characterized using laboratory element tests including triaxial tests [29,32], cyclic direct simple shear tests [30,32], and torsional shear tests [33]. The CDSS tests presented in this study were used in the constitutive model calibration exercise for the 2022 edition of the Liquefaction Experiments and Analysis Project [22-24] where the seismic response of a sheet-pile retaining structure supporting a deposit of Ottawa F65 sand is investigated through a series of centrifuge experiments and numerical simulations performed at different facilities and institutions across the world.

To investigate the effect of density, overburden stress, static shear stress, and cyclic stress ratio on the cyclic strength of Ottawa F65 sand, a relatively large number of experiments was required to cover different relative densities, overburden stresses, and static shear stresses. However, it was realized that other possible relative densities, overburden pressures, and static shear stress values are often needed in numerical modeling of geo-structures. To investigate whether the current CDSS data could be used to estimate the liquefaction strength of Ottawa F65 sand for densities

and loading conditions that are not covered in the experimental results, an Artificial Neural

Networks (ANN) model is developed to predict the soil liquefaction strength for densities and

loading conditions that are not available in the experimental results.

178179

180

181

182

183

184

185 186

187

188

189

161 In recent years, several studies have used Artificial Neural Networks to predict the liquefaction potential of soils based on field data. Goh [34] showed reliability of ANN models in predicting 162 163 liquefaction potential. The study used an ANN model to predict the liquefaction potential using a 164 standard penetration test (SPT) dataset including the SPT value, grain size, percent fines, dynamic 165 shear stress and earthquake magnitude. This model was modified to include cone penetration test 166 (CPT) data [35]. Ali and Najjar [36] have used 61 field data sets from various earthquake sites to 167 train a backpropagation ANN model. The model was validated against 44 records not included in 168 the training data sets. The developed model was shown to outperform fuzzy logic and statistically based approaches. Juang et al. [37] used a dataset collected from cone penetration test (CPT) 169 170 measurements and field observations of liquefaction to train an ANN model with the goal of predicting the occurrence of liquefaction based on soil properties and earthquake loading 171 172 conditions. Predictions of the ANN model were then used to define a liquefaction boundary 173 surface. An empirical equation was associated to the surface by regression analysis. Then, a 174 probabilistic evaluation method of liquefaction potential was developed by conducting probability 175 analyses of the dataset cases using the Bayesian mapping function approach. The simplified method developed by Juang et al. [37] based on CPT data illustrated the suitability of ANN models 176 177 in predicting liquefaction potential.

Artificial Neural Networks were also used in the literature to predict liquefaction strength of sandy soils based on laboratory experiment data. Young-Su and Byung-Tak [38] have developed an ANN model to predict the liquefaction strength of nine clean sands using triaxial and direct simple shear tests results available in the literature. Different combinations of soil parameters were investigated to develop a model with optimum predictions of the number of cycles required for liquefaction triggering. The study has demonstrated applicability of ANN models to soil liquefaction prediction even though these models do not describe the mechanical properties of soils through mathematical equations. The abovementioned studies have selected the training datasets from existing laboratory tests or field data on a particular soil. Hence, the ANN models developed in these studies could only be validated against the existing datasets. A further assessment of the ANN models using the results of new tests that are not known to the predictors would lend additional credibility to the developed models.

190 In this study, the developed ANN model was trained on a dataset of 65 constant volume CDSS 191 tests on Ottawa F65 sand including 54 CDSS tests conducted in the present study and 11 CDSS 192 tests conducted by ElGhoraiby et al. [32]. It is noted that the CDSS tests in this study and the 193 CDSS tests reported by ElGhoraiby et al. [32] were conducted in the same facility following the 194 same procedure. A good agreement between these CDSS tests was obtained in terms of 195 liquefaction strength. The ANN model was trained, validated, and tested to predict the liquefaction 196 strength of Ottawa F65 for a specified set of vertical effective stresses, cyclic stress ratios, static 197 shear stresses and relative densities. The ANN model was further assessed using blind predictions 198 of the liquefaction strength obtained under a new vertical effective stress and a new soil density

that are not included in the training dataset. The blind predictions of the developed ANN model were then validated by carrying out CDSS tests on Ottawa F65 sand under similar density and loading conditions used in the blind predictions.

2. Materials and methods

2.1. Description of Ottawa F65 sand

Ottawa F65 sand is a whole grained white silica sand with a silica purity of 99.7% mined from deposits near Ottawa, Illinois and produced by US Silica [30,32]. Ottawa F65 sand particles are mostly subrounded as shown in Scanning Electron Microscope (SEM) characterization of Ottawa F65 sand (Figure 1). Ottawa F65 sand is selected as the main soil in the Liquefaction Experiments and Analysis Project (LEAP) [22-24]. Previous studies have conducted a series of characterization tests on Ottawa F65 sand to determine its physical and index properties [29-32]. The soil characterization tests included specific gravity of soil particles tests, particle size distribution analysis, hydraulic conductivity tests, and minimum and maximum void ratio tests. Table 1 summarizes the physical and index properties of Ottawa F-65 sand [29,30,32] (D₁₀, D₃₀, and D₆₀ are, respectively, particle diameters defining 10%, 30%, and 60% finer from the grain-size distribution curve, e denotes the void ratio, and e_{max} and e_{min} represent, respectively, maximum and minimum void ratios).



Figure 1: SEM characterization of Ottawa F65 sand.

Physical properties	Vasko (2015)	Bastidas (2016)	ElGhoraiby et al. (2020)				
Specific gravity, G _s	2.65	2.65	2.65				
Particle size distribution							
D ₁₀ (mm)	0.13	0.14	0.136				
D ₃₀ (mm)	0.17	0.17	0.174				
D ₆₀ (mm)	0.21	0.22	0.235				
Coefficient of uniformity, C _u	1.62	1.61	1.728				
Coefficient of curvature, C _c	0.947	0.96	0.96				
Hydraulic conductivity							
Permeability (cm/sec)	0.0118 for $e = 0.639$	0.022 for $e = 0.791$	0.008 to 0.015				
	0.0164 for $e = 0.724$	0.016 for $e = 0.539$	for $e = 0.486$				
			to $e = 0.766$				
Maximum and minimum void ratios							
e _{max}	0.754	0.83	0.78				
e _{min}	0.491	0.51	0.51				

Table 1: Physical and index properties of Ottawa F-65 sand

2.2. Cyclic direct simple shear experimental set up

In this study, multiple series of constant volume stress-controlled cyclic direct simple shear (CDSS) tests were conducted using an SGI type device [39] shown in Figure 2. The equipment includes vertical and horizontal loading rams, and Linear Variable Differential Transformers (LVDT) for vertical and horizontal displacement measurements. The soil specimen is placed between top and bottom caps on which porous stones disks are placed. The soil specimen is enclosed in a rubber membrane and is laterally constrained using a stack of Teflon coated Aluminum rings kept in a vertical position using clevis pins. Figure 2 shows the final set-up of soil specimen.

The top cap is connected to a vertical loading ram via a vertical load cell that allows for precise control of the applied vertical load (precision of 99.8%). The bottom cap is placed on a base pedestal that sits on a shear sliding base. The shear sliding base is connected to a shear loading ram via a horizontal load cell that controls the horizontal displacement applied to the shear base. The bender elements embedded in the top and bottom caps are connected to a wave generating device and enable measurement of shear wave velocity before and after different stages of the CDSS test.

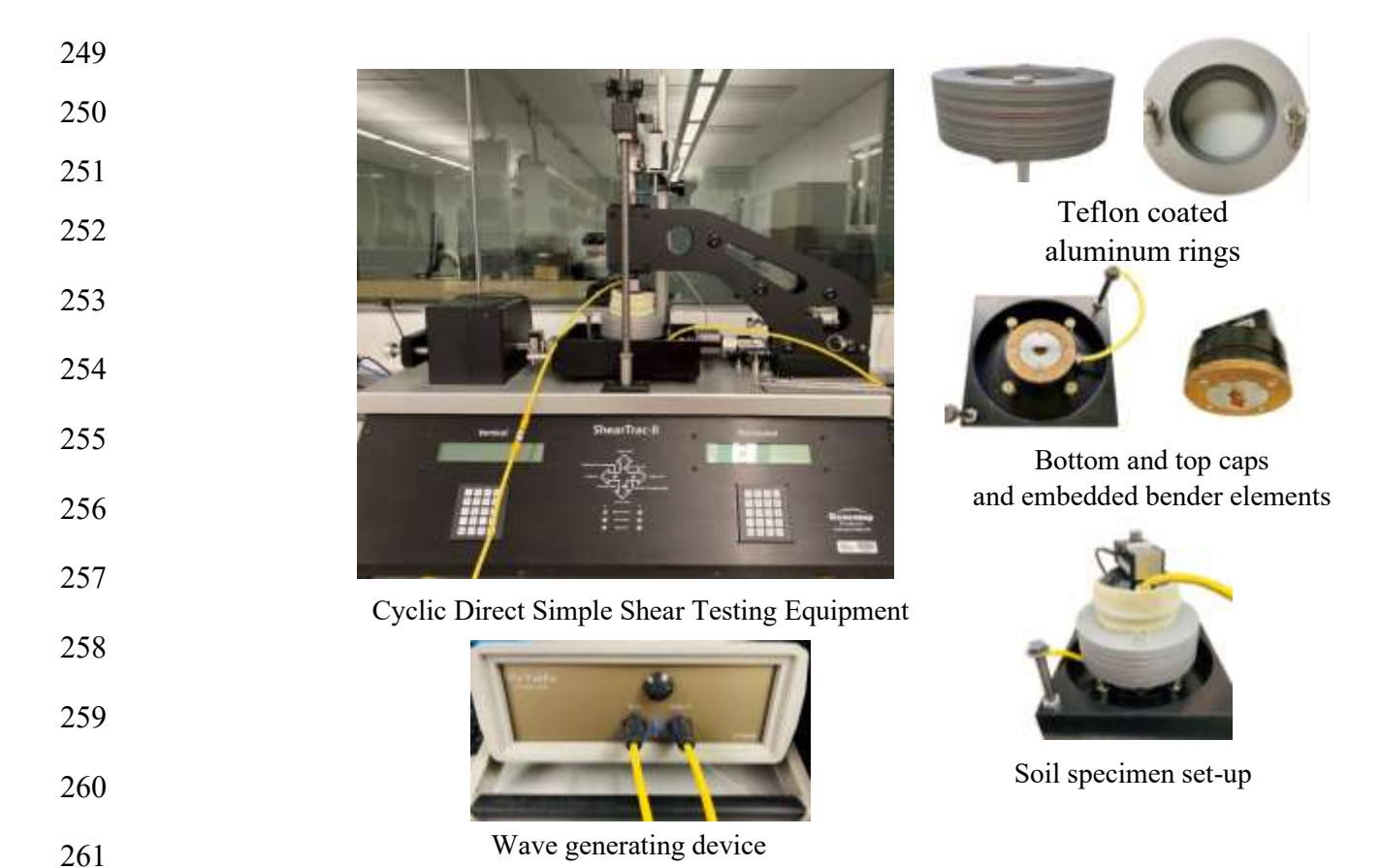


Figure 2: Cyclic direct simple shear experimental set up.

The direct simple shear test usually follows three major steps. First, the soil specimen is prepared following a painstaking procedure to ensure consistency and repeatability of the test results in terms of measured soil density and soil stress-strain behavior. Second, the soil specimen is subjected to a vertical (consolidation) stress. Third, a monotonic or cyclic shear stress is applied to the soil specimen in the horizontal direction. In the case of tests with static shear stress, a precyclic shearing stage is added to the third step.

In this study, the samples were prepared using dry pluviation technique. The dry pluviator shown in Figure 3 is composed of a 1-inch diameter tube connected to a bucket at its top. A sieve number 8 covers the bottom of the tube. The tube is supported by a pluviator lift attached to a steel frame through a threaded rod that can have upwards and downwards movements controlled by a DC motor connected to a power supply. A height measuring ruler with graduations in millimeter is attached to the steel frame to indicate the height of drop.

In sample preparation, the soil density is conditioned by the height of drop. Depending on the target density, an initial height of drop is determined by trial and error and the pluviator lift is positioned at that height. Then, sand is deposited in the upper bucket and upward movement is imposed on the pluviator lift at a constant speed in order to maintain a constant height of drop. The sand is gradually collected inside the stacked rings covered by the rubber membrane as shown in Figure 4. Attention is given to the symmetry of the deposited sample as it conditions the symmetry

of the stress-strain response under cyclic loading. When the sand fills the volume inside the stack of rings and overflows from the surface, the upward movement of the pluviator lift is stopped. The excess sand is collected in the sand collector. The sample surface is then leveled as shown in Figure 4.

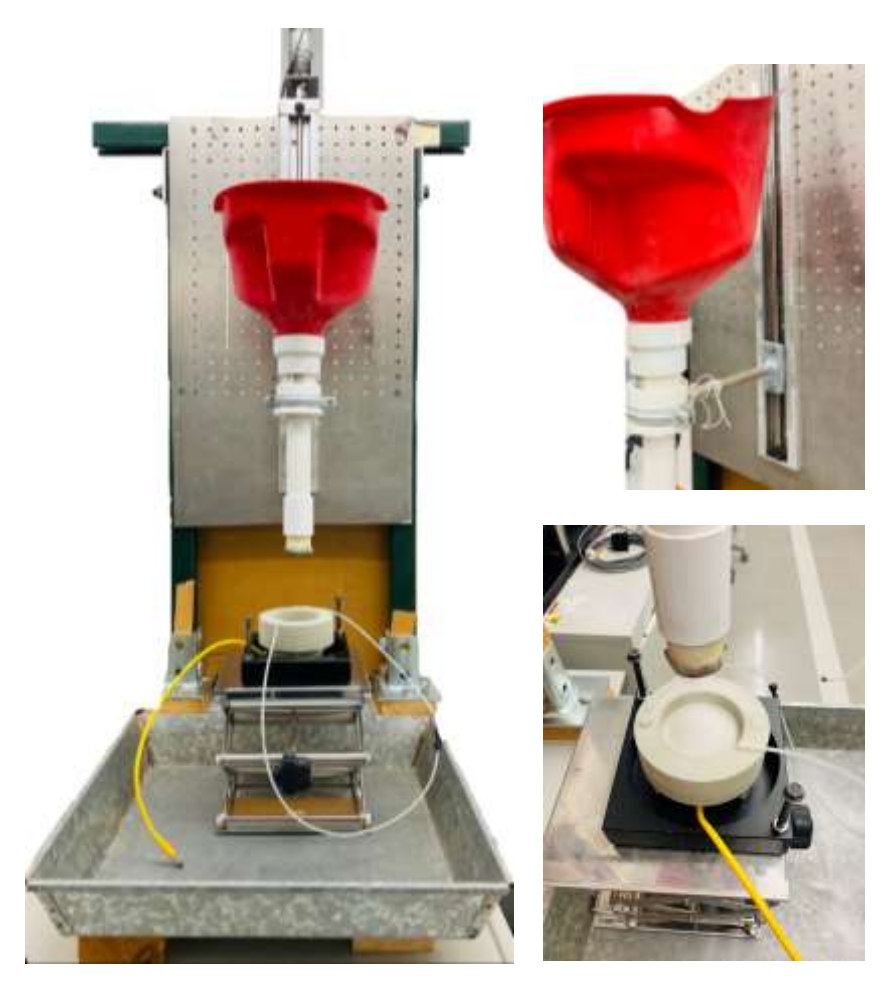


Figure 3: Constant height dry pluviation station.

285

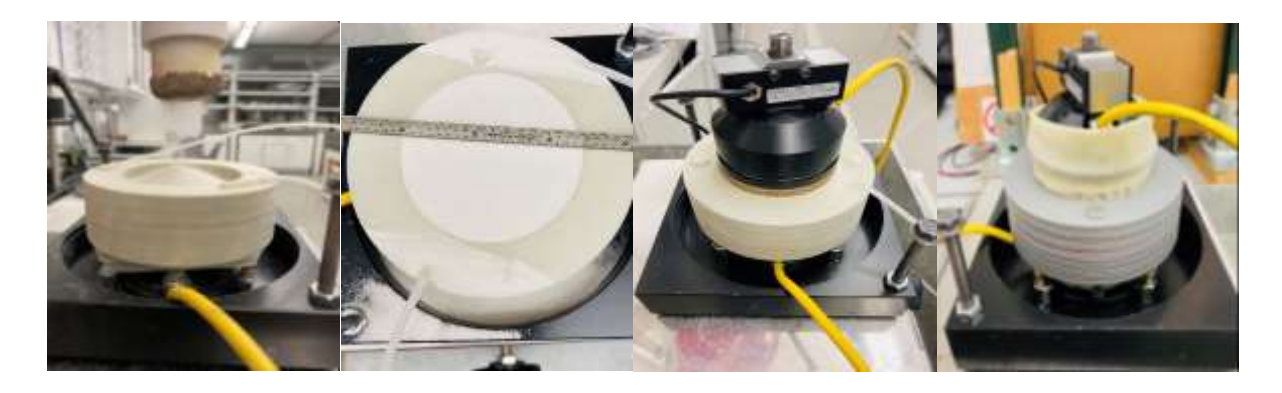


Figure 4: Direct simple shear sample preparation steps after dry pluviation.

Measurements of the height and diameter of the volume that will be occupied by the cylindrical soil specimen are taken at four different locations before dry pluviation. For each specimen, the average height and diameter are obtained, and the specimen volume is calculated. At the end of sample preparation, the specimen surface is leveled as shown in Figure 4. After vacuuming the extra sand on the edges, the weight of the soil specimen with the base pedestal, stack of rings, membrane, and O-rings is measured. The weight of soil specimen is obtained by subtracting the weight of the base pedestal, stack of rings, membrane, and O-rings. The soil density is calculated from the measured volume occupied by sand and the measured weight of sand collected inside the stack of rings after leveling the specimen surface. By ensuring consistency in the specimen preparation approach and maintaining the same height of drop in dry pluviation, soil specimens are prepared with a relatively small variation in relative density (coefficients of variation less than 2% for target relative densities used in this study). Considering all constant volume direct simple shear tests conducted in this study, the average specimen height was estimated at 23.5 mm with a coefficient of variation of 0.45%, and the average specimen diameter was estimated at 64.2 mm with a coefficient of variation of 0.05%. In this study, four target relative densities were considered ranging from 55% to 75%. The weight of soil specimen varied with increased target relative density. The average coefficient of variation of soil specimen weight was estimated at 0.59%.

During the constant volume CDSS tests, the lateral displacement of the soil specimen is constrained using the stack of Teflon coated Aluminum rings. As mentioned earlier, the soil specimen is placed between top and bottom caps on which porous stones disks are positioned. The vertical displacement is unconstrained during the consolidation phase. Before shearing, the vertical displacement is locked using a passive control system that prevents the development of axial strain during shearing. The constant volume condition is ensured through the constrained lateral and vertical displacements during shearing.

310 3. Results and Discussion

286

287

288

289

290

291

292

293

294

295

296

297

298

299

300

301

302

- In this study, a total of fifty-four CDSS tests were conducted for a set of overburden stresses,
- 312 relative densities, static shear stresses, and cyclic stress ratios to demonstrate the effect of these
- parameters on the soil cyclic strength. The relative densities for each test are calculated based on
- a maximum void ratio of 0.78 and a minimum void ratio of 0.51 used in the LEAP 2017 [31,24].
- In each CDSS test, the soil specimen was loaded to a maximum shear strain of 10% in double
- amplitude using stress control criterion for load reversal.

3.1. Cyclic direct simple shear tests results

318 3.1.1. Effect of overburden stress on cyclic strength of Ottawa F65

- Two series of constant volume CDSS tests were conducted under overburden stresses of 40 kPa
- and 100 kPa on specimens prepared at average relative densities of 66.2% (covariance of 0.8%)
- and 66.7% (covariance of 1.4%), respectively. These tests complement the experiments conducted
- 322 by ElGhoraiby et al. [32] by considering higher cyclic stress ratios. Table 2 summarizes
- information about the average dry density before consolidation (ρ_d), average void ratio after
- 324 consolidation (e_{ac}), average relative density after consolidation (D_{r,ac}) for the two sets of CDSS

tests subjected to vertical stresses (σ'_v) of 40 kPa and 100 kPa. The ranges of cyclic stress ratios (CSR) and ranges of the measured number of cycles required to reach 3.5%, 5%, and 7.5% double amplitude (DA) shear strain (Ncyc – 3.5%, Ncyc – 5%, Ncyc – 7.5%) are reported in the Table. In these tests, the specimens were not subjected to static initial shear stress. Hence, the static shear stress ratio α (defined as the ratio of static initial shear stress to initial vertical effective stress) is zero.

$\sigma'_{v}=40~kPa~, \alpha=0$										
$\rho_{d} \left(kg/m^{3} \right) \hspace{0.2cm} e_{ac} \hspace{0.2cm} D_{r,ac} (\%) \hspace{0.2cm} CSR \hspace{0.2cm} Ncyc - 3.5\% \hspace{0.2cm} Ncyc - 5\% \hspace{0.2cm} Ncyc - 7.5\%$										
1641	0.601	66.2	0.15 - 0.25	1 - 26	1.5 - 28	2 - 32.5				
	$\sigma'_{v} = 100 kPa , \alpha = 0$									
1628	0.600									

Table 2: Summary of constant volume CDSS tests with $\sigma'_v = 40$ kPa, 100 kPa.

For each CDSS test, shear wave velocity measurements were taken after the consolidation phase and before cyclic shearing using the bender element and wave generating device shown in Figure 2. At the end of consolidation, a shear wave is transmitted using the wave generating device. Figure 5 presents the transmitted and received shear wave time history for a test conducted under a vertical stress of 40 kPa. The departure and arrival time of the shear wave are recorded. The time difference between departure and arrival is calculated (peak to peak time difference). Then, the shear wave velocity is computed knowing the distance traveled by the wave. The shear modulus G is computed using the equation $G = \rho V_s^2$ where ρ is the soil density and V_s is the shear wave velocity. The peak-to-peak time difference recorded in Figure 5 is 82.8 μ s, which corresponds to a calculated shear modulus of 35.5 MPa.

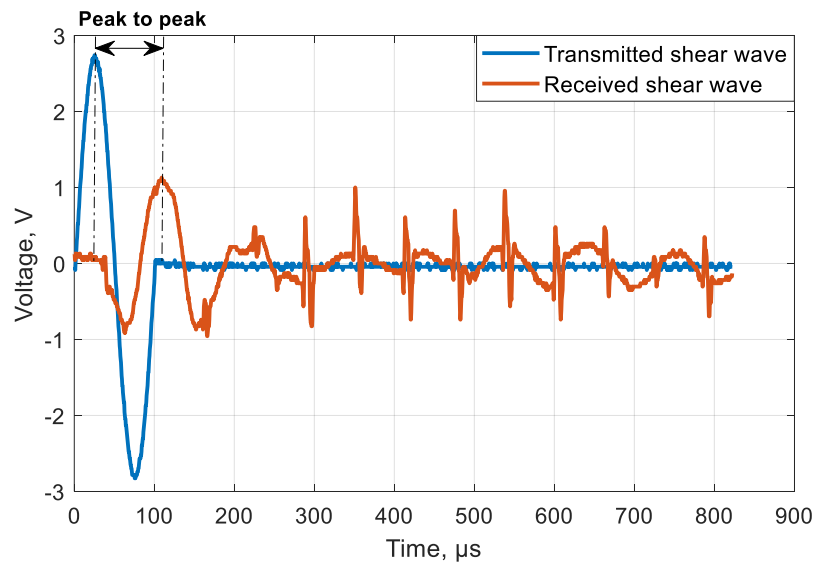


Figure 5: Example of transmitted and received shear wave.

Table 3 summarizes the average shear wave velocity and average shear modulus for CDSS tests conducted under vertical stresses (σ'_n) of 40 kPa and 100 kPa.

/ (I.D.)	Shear wave v	velocity, V_s	Shear modulus, <i>G</i>		
σ'_{v} (kPa)	Mean (m/s)	COV (%)	Mean (MPa)	COV (%)	
40	147.3	2.9	35.7	5.8	
100	157.5	2.3	40.6	4.9	

Table 3: Shear wave velocity and shear modulus for constant volume CDSS tests with $\sigma'_{v} = 40 \text{ kPa}$ and $\sigma'_{v} = 100 \text{ kPa}$.

Figure 6 shows results of two CDSS tests conducted at vertical stresses of 40 kPa and 100 kPa on soil samples prepared at a relative density of about 66.7% in average. The specimens were subjected to cyclic shearing at a cyclic stress ratio (CSR) of 0.20 under constant volume condition. Figure 6 presents the variation of shear stress with shear strain, the stress path (shear stress variation with vertical stress), and the variation of vertical effective stress and vertical effective stress ratio (vertical effective stress divided by initial vertical effective stress) with the number of cycles. The stress-strain response shows that the double amplitude shear strain increases as the soil weakens and deforms more with every additional cycle. The stress path response shows that the soil specimen contracts first under the applied shear stress, which corresponds to soil tendency to decrease in volume. Since the test is conducted under constant volume criteria, the vertical stress decreases to maintain a constant specimen height. Then, the soil contracts and then dilates at the end of each forward and backward loading as the soil resists shearing through dilation or volume expansion. As the vertical effective stress ratio approaches a near zero value, the contact stresses between soil particles momentarily approach zero and large strains develop in the soil.

The test conducted under 40 kPa vertical stress has required a larger number of cycles for the vertical effective stress to reach a near zero value. It is also observed that a larger number of cycles was required to reach 10% double amplitude shear strain in the CDSS test conducted under a vertical stress of 40 kPa compared to the test conducted under a vertical stress of 100 kPa. Since the specimens in the two tests were subjected to the same cyclic stress ratio and have close relative densities, it is clear that cyclic strength increases with decreased overburden stress.

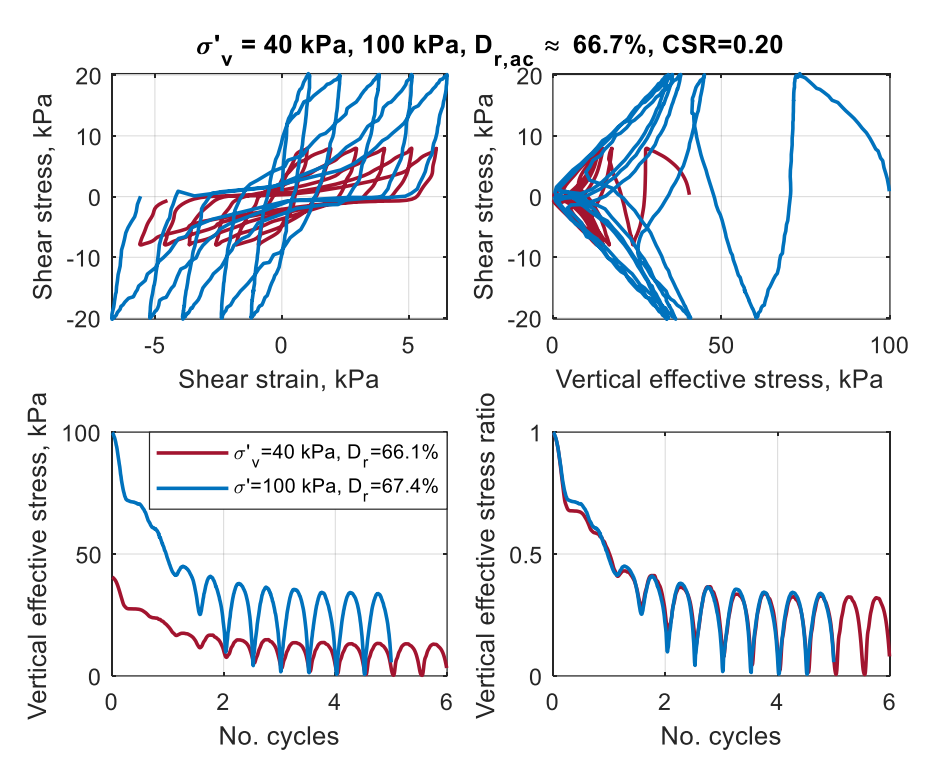


Figure 6: Constant volume stress controlled CDSS tests results, $\sigma'_v = 40 \text{ kPa}$, 100 kPa, $D_{r,ac} \approx 66.7\%$, CSR = 0.20.

Figure 7 presents the liquefaction strength curves obtained using the two series of constant volume CDSS tests conducted under overburden stresses of 40 kPa and 100 by considering the number of cycles required to reach 7.5% double amplitude shear strain. It is noted that, for similar density and cyclic stress ratio, a larger number of cycles is required for tests conducted under an overburden stress of 40 kPa to reach the same shear strain amplitude. The liquefaction strength curves shown in Figure 7 follow the general form $CSR = a \times Ncyc^{-b} + c$ where a, b, and c are constant parameters. This form was more convenient to capture all datapoints covering cyclic stress ratios used in this study as well as those used by ElGhoraiby et al. [32]. Table 4 summarizes the constant parameters for the liquefaction strength curves shown in Figure 7.

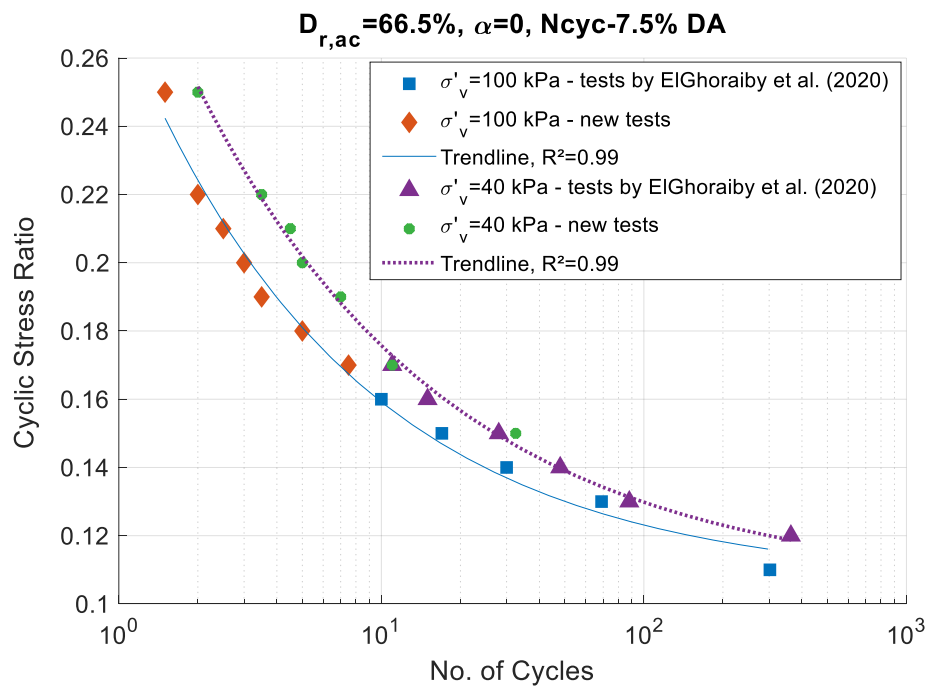


Figure 7: Liquefaction strength curves for constant volume CDSS tests with $\sigma'_{v} = 40 \ kPa$ and $100 \ kPa$, and $D_{r,ac} \approx 66.5\%$.

Vertical stress σ'_v , kPa	$D_{r,ac}$, %	Parameter a	Parameter b	Parameter c
40	66.2	0.20	0.45	0.105
100	66.7	0.17	0.49	0.106

Table 4: Liquefaction strength curves constant parameters for constant volume CDSS tests with $\sigma'_v = 40$ kPa, 100 kPa and Ncyc-7.5% double amplitude shear strain.

Idriss and Boulanger [9] have developed a correction factor K_{σ} for sandy soils to account for the increase in strength due to the decrease in confining stress based on the strength of the soil tested at a confining stress of 100 kPa. The correction factor K_{σ} is defined by the equation $K_{\sigma} = 1 - C_{\sigma} \ln\left(\frac{\sigma'v_0}{P_a}\right)$ where $\sigma'v_0$ is the effective overburden stress, P_a is the atmospheric pressure, and C_{σ} is a coefficient used to correlate soil relative density D_r , SPT N-values $(N_{1,60})$ and CPT tip resistance $(q_{c,1,N})$ to K_{σ} . The high overburden correction, K_{σ} , accounts for the increased susceptibility of sandy soils to cyclic liquefaction with increased effective overburden stress at the same cyclic stress ratio.

Table 5 presents the average values of K_{σ} calculated for the two series of CDSS tests conducted under overburden stresses of 40 kPa and 100 kPa. The correction factor K_{σ} is compared to the experimental ratio of cyclic resistance ratio (CRR) values CRR_{40}/CRR_{100} (where CRR_{40} and CRR_{100} correspond, respectively, to CRR values for tests conducted under vertical stresses of 40 and 100 kPa) calculated for a moment magnitude of earthquake M=7.5, which corresponds to cyclic strength at 15 uniform stress cycles [13]. The measured ratio of the CRR values (CRR_{40}/CRR_{100}) obtained from the two series of CDSS tests is slightly higher (3.8% higher) than the correction factor K_{σ} calculated from the relationship proposed by Boulanger and Idriss [9]. This is consistent

with the observations made by Park et al. [12] who have measured the correction factor K_{σ} in a series of CDSS tests conducted on loose and dense specimens of Nakdong River sand. The study by Park et al. [12] suggested that the correction factor K_{σ} by Boulanger and Idriss [9] provides effective predictions for loose sand compared to the measured correction factor [12]. However, the correction factor K_{σ} provided significantly lower predictions for dense sand compared to the measured ratio of CRR values. It was also found that the predicted correction factor K_{σ} is only effective for cases where the initial static shear stress is insignificant.

σ'_{v} (kPa)	σ'_v/P_a	$D_{r,ac}$, %	C_{σ}	K_{σ}	$CRR_{\sigma'_{v}}/CRR_{\sigma'_{v}=100\ kPa}$
40	0.39	66.22	0.134	1.05	1.09
100	0.99	66.69	0.136	1.00	1.00

Table 5: High Overburden Correction factor K_{σ} and CRR ratio at M=7.5.

3.1.2. Effect of static shear stress on cyclic strength of Ottawa F65

402 403

404

405

406 407

408

409

410

411

412

413

414

415 416

417 418

419

420

421 422

423

424

425

426

427

428

429 430

The effect of static shear stress on the cyclic strength of Ottawa F65 sand was studied by conducting four different series of constant volume CDSS tests where the soil specimen is subjected to a static shear stress after consolidation and prior to cyclic shearing. The application of a static shear stress after consolidation replicates the condition of sloping ground where any element under the ground surface is under a shear stress in addition to vertical and horizontal stresses. The constant volume CDSS tests with static shear stress include two sets of tests with a consolidation stress (σ'_{ν}) of 100 kPa and static shear stress ratios (α) of 0.3 and 0.4, and two sets of tests with a consolidation stress of 40 kPa and static shear stress ratios of 0.25 and 0.375. Table 6 shows the average dry density before consolidation (ρ_d), void ratio after consolidation (eac) and relative density after consolidation (Dr,ac) for the different sets of CDSS tests conducted with static shear stress. The ranges of cyclic stress ratio and ranges of the measured number of cycles required to reach 3.5%, 5%, and 7.5% double amplitude (DA) shear strain (Ncyc -3.5%, Ncyc -5%, Ncyc -7.5%) are reported in Table 6. It is noted that, for constant volume CDSS tests conducted under a vertical effective stress of 100 kPa and static shear stress ratios of 0.3 and 0.4, the shear strain amplitude has not reached a value of 7.5% under the applied cyclic stress ratios. In these cases, the soil specimens did not reach a state of liquefaction and stress paths stabilized at a vertical stress higher than zero.

	$\sigma'_{v}=100~kPa$, $lpha=0.3$									
$\rho_{\rm d}({\rm kg/m^3})$	e _{ac}	D _{r,ac} (%)	CSR	Ncyc - 3.5%	Ncyc – 5%	Ncyc – 7.5%				
1641	0.602	66.5	0.15 - 0.30	1 - 35	2 - 90	-				
	$\sigma'_{v}=100~kPa$, $\alpha=0.4$									
1637	0.602	67.7	0.15 - 0.30	2 - 48	5 - 126	-				
			$\sigma'_{v} = 40 k$	αPa , $\alpha = 0.25$						
1640	0.601	66.4	0.20 - 0.30	1.5 - 11	2.5 - 24.5	5 - 67				
$\sigma'_{v} = 40 \ kPa$, $\alpha = 0.375$										
1638	0.601	66.4	0.22 - 0.35	4 - 24	7.5 - 74	15 - 280				

Table 6: Summary of constant volume CDSS tests with $\sigma'_v = 100 \ kPa$, $\alpha = 0.3$, 0.4 and $\sigma'_v = 40 \ kPa$, $\alpha = 0.25$, 0.375.

Figure 8 presents results of three constant volume CDSS tests conducted at a vertical stress of 100 kPa and subjected to static shear stresses of 0 kPa, 30 kPa, and 40 kPa prior to cyclic shearing under a constant volume condition with a cyclic stress ratio of 0.25. The three specimens were prepared at nearly the same relative density. It is noticed that for tests with static shear stress, the soil specimen does not reach a state of liquefaction and stabilizes at a vertical stress that is higher for cases with larger static shear stress ratio. While the soil specimen subjected to no static shear stress has reached a near zero vertical effective stress ratio, the soil specimens subjected to static shear stresses of 30 kPa and 40 kPa have stabilized at vertical effective stresses of 60 kPa and 95 kPa, respectively. It is also noted that a larger number of cycles is required to reach 5% double amplitude shear strain amplitude with increased values of static shear stress.

Figure 9 presents the liquefaction strength curves corresponding to the abovementioned series of CDSS tests conducted with static shear stress in addition to the series of tests conducted without static shear stress and described in previous sections. The Figure shows that the cyclic strength increases with larger static shear stress for both series of CDSS tests conducted under overburden stresses of 100 kPa and 40 kPa. Table 7 summarizes the constant parameters of the liquefaction strength curves of general form $CSR = a \times Ncyc^{-b} + c$ (where a, b, and c are constant parameters) for the liquefaction strength curves shown in Figure 9.

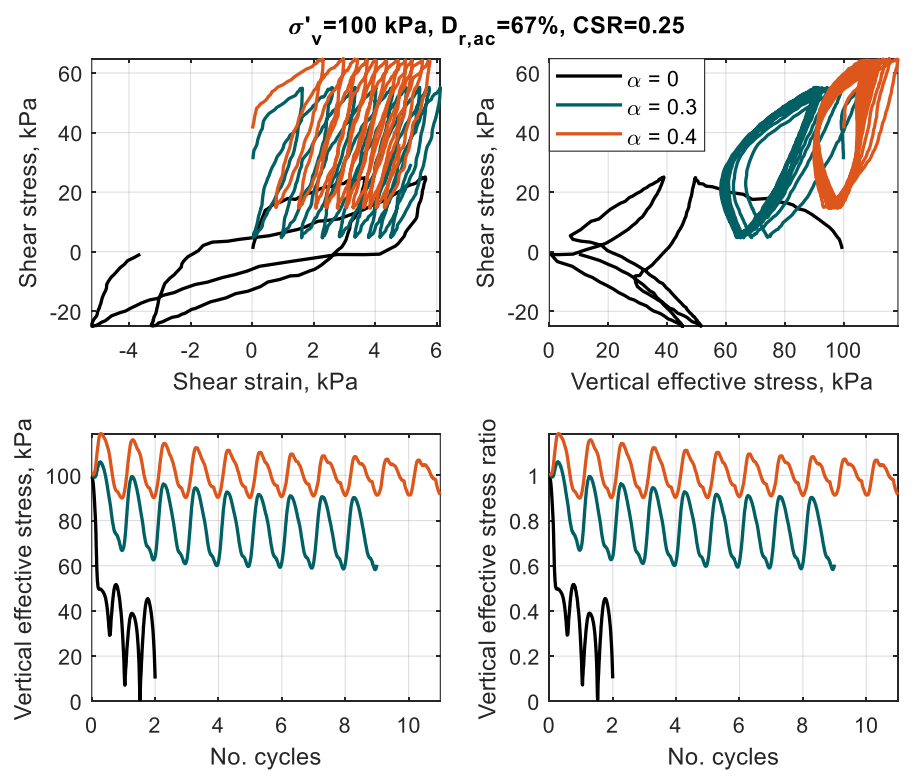


Figure 8: Constant volume CDSS test results $-\sigma'_v = 100 \ kPa$, $\alpha = 0$, 0.3, 0.4, CSR = 0.25, $D_{r,ac} \approx 67\%$.

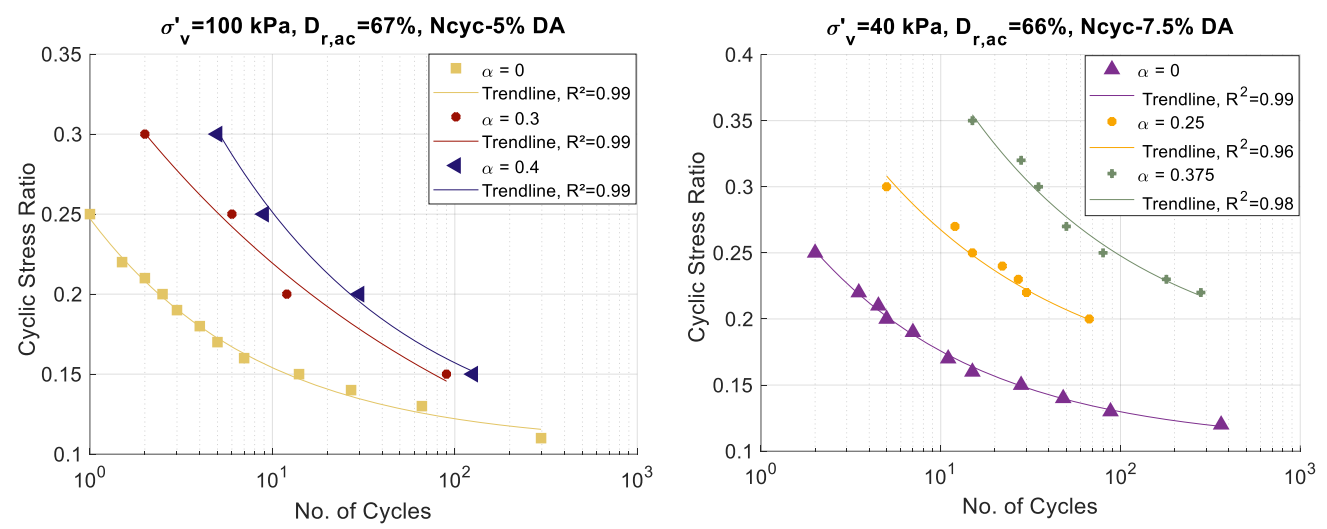


Figure 9: Liquefaction strength curves for CDSS tests with $\sigma'_v = 100 \, kPa$, $\alpha = 0, 0.3, 0.4$ (left) and $\sigma'_v = 40 \, kPa$, $\alpha = 0, 0.25, 0.375$ (right).

Vertical stress σ'_{v} , kPa	α	$D_{r,ac}$, %	Parameter a	Parameter b	Parameter c
40	0	66.2	0.20	0.45	0.105
40	0.25	66.4	0.32	0.40	0.140
40	0.375	66.4	0.61	0.43	0.160
100	0	66.7	0.17	0.49	0.106
100	0.3	67.1	0.32	0.22	0.024
100	0.4	67.1	0.39	0.41	0.097

Table 7: Liquefaction strength curves constant parameters for constant volume CDSS tests with $\sigma'_v = 40 \ kPa$, Ncyc-7.5% shear strain, and $\sigma'_v = 100 \ kPa$, Ncyc-5% shear strain.

To account for the effect of static shear stress ratio on the liquefaction strength of sandy soils, a correction factor K_{α} is often used where α is the ratio of static shear stress to vertical (consolidation) stress [9]. The correction factor K_{α} is defined as the ratio of CRR for a non-zero value of α to the CRR for $\alpha=0$. The correction factor K_{α} is related to soil relative density D_r and is also correlated with normalized SPT N-values ($N_{1,60}$) and CPT tip resistance ($q_{c,1,N}$). Boulanger [11] has introduced a state-dependent index for describing the variation of K_{α} with both relative density and confining stress. Table 8 shows the average values of K_{α} calculated for the series of CDSS tests and their comparison with the experimental ratio of the CRR values ($CRR_{\alpha}/CRR_{\alpha=0}$) calculated for a moment magnitude of earthquake M=7.5, which corresponds to cyclic strength at 15 uniform stress cycles [13]. Figure 10 compares the empirical K_{α} versus the experimental ratio of the CRR values ($CRR_{\alpha}/CRR_{\alpha=0}$) for vertical effective stresses of 40 kPa and 100 kPa. Compared to the experimental results shown in Figure 10, the empirical equations [8,10] provide larger values of K_{α} to account for the effect of static shear stress. These observations appear to be consistent with those made by Park et al. [12]. It is noted, however, that the empirical equations were developed from data for which the static shear stress ratio α is less than 0.3.

σ'_{v} (kPa)	τ (kPa)	α	$D_{r,ac}(\%)$	$(N_1)_{60}$	q_{c1N}	K_{α}	CRR_{α}
							$/CRR_{\alpha=0}$
40	0	0	66.2	20.2	129.3	1.00	1.00
40	10	0.25	66.4	20.3	129.8	1.84	1.52
40	15	0.375	66.4	20.3	129.7	2.20	2.16
100	0	0	66.7	20.5	130.6	1.00	1.00
100	30	0.3	66.5	20.4	130.2	1.79	1.39
100	40	0.4	67.7	21.1	133.5	2.31	1.56

Table 8: Static shear stress ratio Correction factor K_{α} and experimental ratio of CRR at M=7.5 for $\sigma'_{\nu} = 40 \ kPa$ and $\sigma'_{\nu} = 100 \ kPa$.

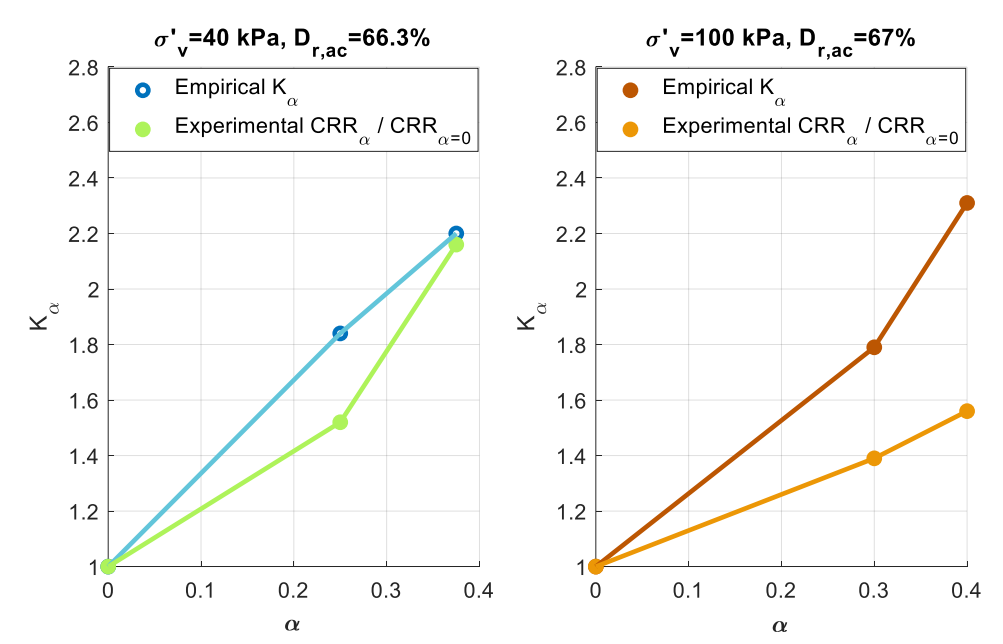


Figure 10: Static shear stress ratio Correction factor K_{α} and experimental ratio of CRR at M=7.5 for $\sigma'_{\nu} = 40 \ kPa$ and $\sigma'_{\nu} = 100 \ kPa$.

3.1.3. Effect of soil density on cyclic strength of Ottawa F65

The effect of soil density on the cyclic strength of Ottawa F65 soil is studied by conducting multiple series of constant volume CDSS tests on Ottawa F65 sand specimens consolidated at a vertical stress of 40 kPa and prepared at average relative densities after consolidation of 55.2%, 71.2%, and 75.5% in addition to the tests conducted at a relative density after consolidation of 66.2% discussed in the previous section.

Table 9 summarizes the average dry density before consolidation (ρ_d), void ratio after consolidation (e_{ac}) and relative density after consolidation ($D_{r,ac}$) for the different sets of CDSS tests subjected to a vertical stress of 40 kPa and conducted on specimens prepared at three target relative densities after consolidation of 55%, 71%, and 75%. The ranges of cyclic stress ratio and ranges of the measured number of cycles required to reach 3.5%, 5%, and 7.5% double amplitude (DA) shear strain (Ncyc – 3.5%, Ncyc – 5%, Ncyc – 7.5%) are reported in the Table.

	$\sigma'_{v} = 40 \ kPa \ , \alpha = 0$										
$\rho_{d} \left(kg/m^{3} \right) e_{ac} D_{r,ac} (\%) \qquad CSR \qquad Ncyc - 3.5\% \qquad Ncyc - 5\% \qquad Ncyc - 7.5$											
1611	0.631	55.2	0.10 - 0.19	2.5 - 107	3 - 110	4.5 - 115					
1656	0.588	71.2	0.15 - 0.23	2.5 - 51	3 - 54	5 - 58					
1667	0.576	75.5	0.16 - 0.30	1 - 44.5	1 - 47	2 - 49					

Table 9: Summary of constant volume CDSS tests with $\sigma'_v = 40 \text{ kPa}$ and $D_{r,ac} = 55.2\%, 71.2\%, 75.5\%$.

Figure 11 presents the results of three constant volume CDSS tests on soil specimens prepared at three different soil densities (55%, 66.1%, and 75.9%). The specimens are consolidated under a vertical stress of 40 kPa and then subjected to a cyclic stress ratio of 0.19. The stress-strain responses show that, for each cycle, the shear strain amplitude is larger for specimens with lower relative density. The stress paths (shear stress variation with vertical stress) indicate that soil specimens with lower density are more contractive as their vertical stress decreases faster. A smaller number of cycles is required for the vertical stress to approach zero for looser specimens.

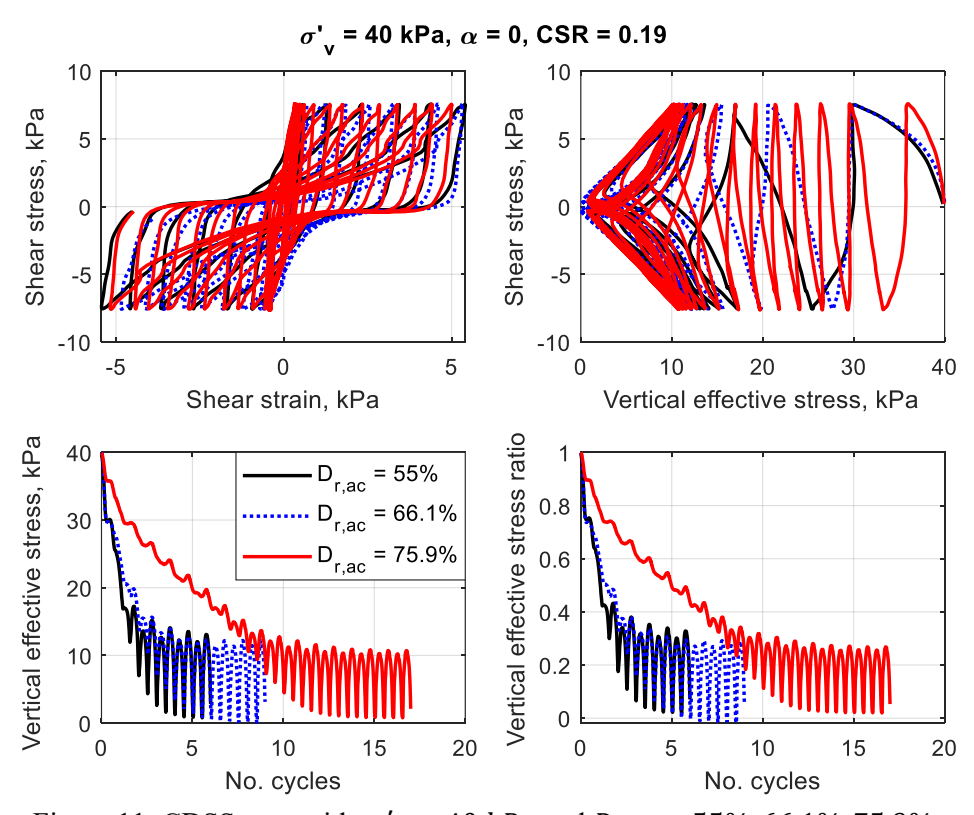


Figure 11: CDSS tests with $\sigma'_{v} = 40 \text{ kPa}$ and $D_{r,ac} = 55\%$, 66.1%, 75.9%.

Figure 12 presents the liquefaction strength curves obtained using the four series of CDSS tests by considering the number of cycles required to reach 7.5% double amplitude shear strain. As expected, cyclic strength of the soil increases with increased density.

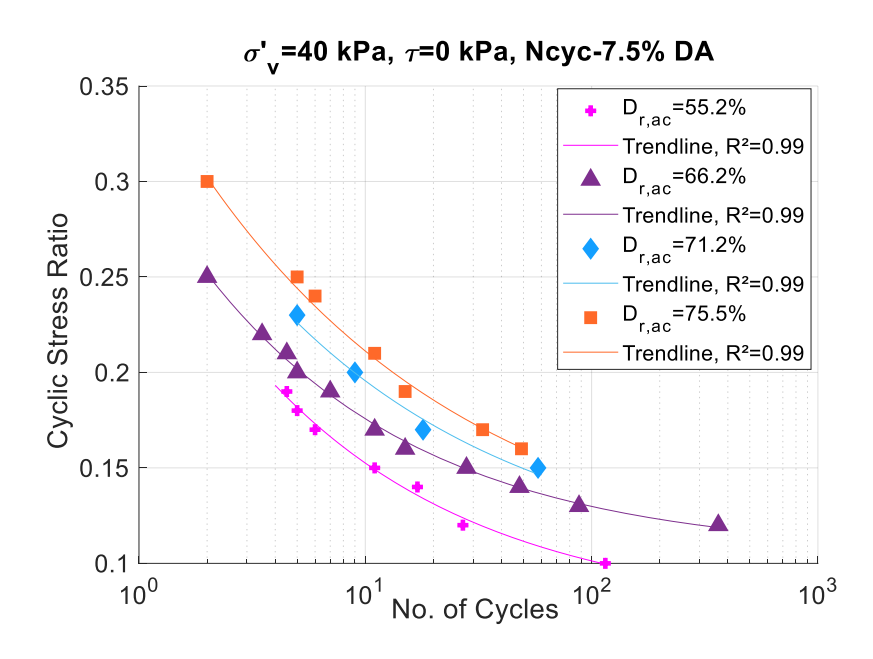


Figure 12: Liquefaction strength curves for CDSS tests with $\sigma'_v = 40 \text{ kPa}$ and $D_{r,ac} = 55.2\%$, 66.2%, 71.2%, 75.5%.

Table 10 summarizes the constant parameters of the liquefaction strength curves of general form $CSR = a \times Ncyc^{-b} + c$ (where a, b, and c are constant parameters) for the liquefaction strength curves shown in Figure 17. The values of the parameter b are similar for tests conducted with soil relative densities of 55.2% and 66.2%. The parameter b decreases with increasing soil density for the series of tests conducted with soil relative densities of 71.2% and 75.4%. It is noted that approximately 19% increase in cyclic strength (CRR corresponding to 15 uniform cycles) is observed when the soil relative density is increased by 10%.

Vertical stress σ'_{v} , kPa	α	$D_{r,ac}$, %	Parameter a	Parameter b	Parameter c
40	0	55.2	0.22	0.45	0.073
40	0	66.2	0.20	0.45	0.105
40	0	71.2	0.24	0.39	0.096
40	0	75.4	0.27	0.36	0.094

Table 10: Liquefaction strength curves constant parameters for constant volume CDSS tests with $\sigma'_v = 40 \ kPa$ and $D_{r,ac} = 55.2\%$, 66.2%, 71.2%, 75.4%.

For these series of tests, shear wave velocity measurements were taken after the consolidation phase and before cyclic shearing using the wave generating device shown in Figure 2. Table 11 summarizes the average shear wave velocity and average shear modulus for CDSS tests conducted under vertical stresses of 40 kPa at average relative densities of 55.2%, 66.2%, 71.2%, and 75.4%.

D (0/)	Shear wave vo	elocity, V _s	Shear modulus, <i>G</i>		
$D_{r,ac}(\%)$	Mean (m/s)	COV (%)	Mean (MPa)	COV (%)	
55.2	131.8	3.9	28.0	7.6	
66.2	147.3	2.9	35.7	5.8	
71.2	151.5	2.6	38.0	5.3	
75.4	158.6	2.7	41.9	5.4	

Table 11: Shear wave velocity and shear modulus for constant volume CDSS tests with $\sigma'_{\nu} = 40$ kPa and $D_{r} = 55.2\%$, 66.2%, 71.2%, 75.4%.

Figure 13 presents the variation of shear wave velocity and shear modulus with relative density for tests conducted at a vertical stress of 40 kPa. Each boxplot indicates the median shear modulus represented by the central mark, as well as the 25th and 75th percentiles represented by the bottom and top edges respectively. Overall, it is observed that the shear wave velocity and shear modulus increase with increased relative density.

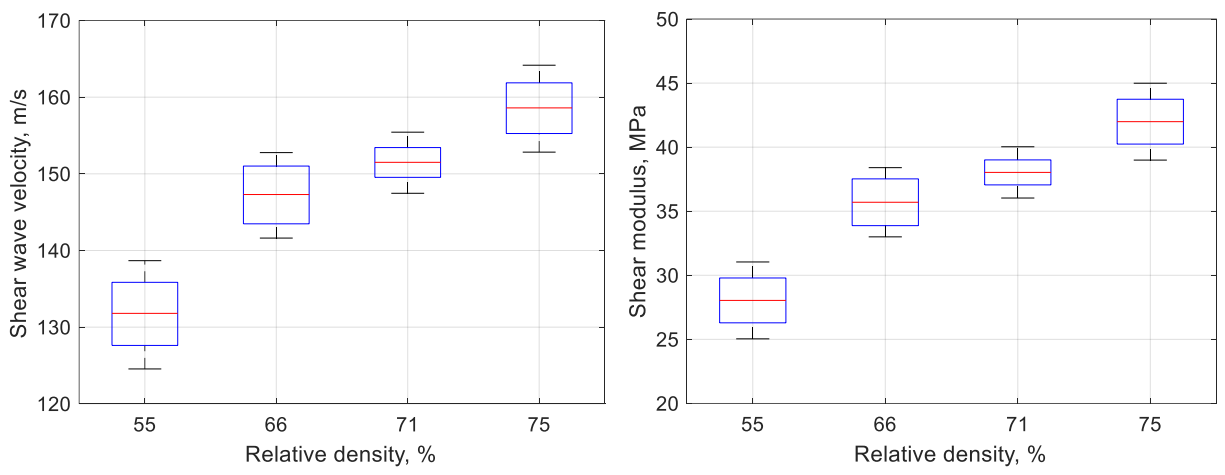


Figure 13: Shear wave velocity versus relative density (left) and shear modulus versus relative density (right).

3.2. Approximation of Ottawa F65 cyclic strength using surface plots

In the CDSS tests presented in previous sections, four varying parameters were considered: soil density, vertical stress, static shear stress, and cyclic stress ratio. For every set of CDSS tests, one parameter was constant while the three other parameters were changing. In order to approximate the cyclic strength of Ottawa F65 sand for values of the varying parameters not available in the experimental data, a surface fitting tool for three-dimensional data was used to approximate the variation of number of cycles with cyclic stress ratio and relative density, or the variation of number of cycles with cyclic stress ratio and static shear stress. The surface fitting tool used is a Python open-source code that fits the experimental data against multiple functions, and then provides a ranking of the functions by considering the highest to the lowest coefficient of determination R^2 . The Python open-source code is available at Bitbucket Git-based source code repository [40]. The code uses a genetic algorithm for initial parameter estimation [41] and includes orthogonal distance and relative error regressions [42].

Figure 14 presents surface plots used to fit the variables considered in the different sets of CDSS tests conducted in this study. Figure 14 describes:

- (1) The variation of the number of cycles to reach 5% shear strain with cyclic stress ratio (CSR) and static shear stress ratio (α) for CDSS tests conducted under a vertical stress of 100 kPa (graph 1).
- (2) The variation of the number of cycles to reach 7.5% shear strain with cyclic stress ratio (CSR) and static shear stress ratio (α) for CDSS tests conducted under a vertical stress of 40 kPa (graph 2).
- (3) The variation of the number of cycles to reach 7.5% shear strain with cyclic stress ratio (CSR) and relative density after consolidation $D_{r,ac}$ for CDSS tests conducted under a vertical stress of 40 kPa (graph 3).

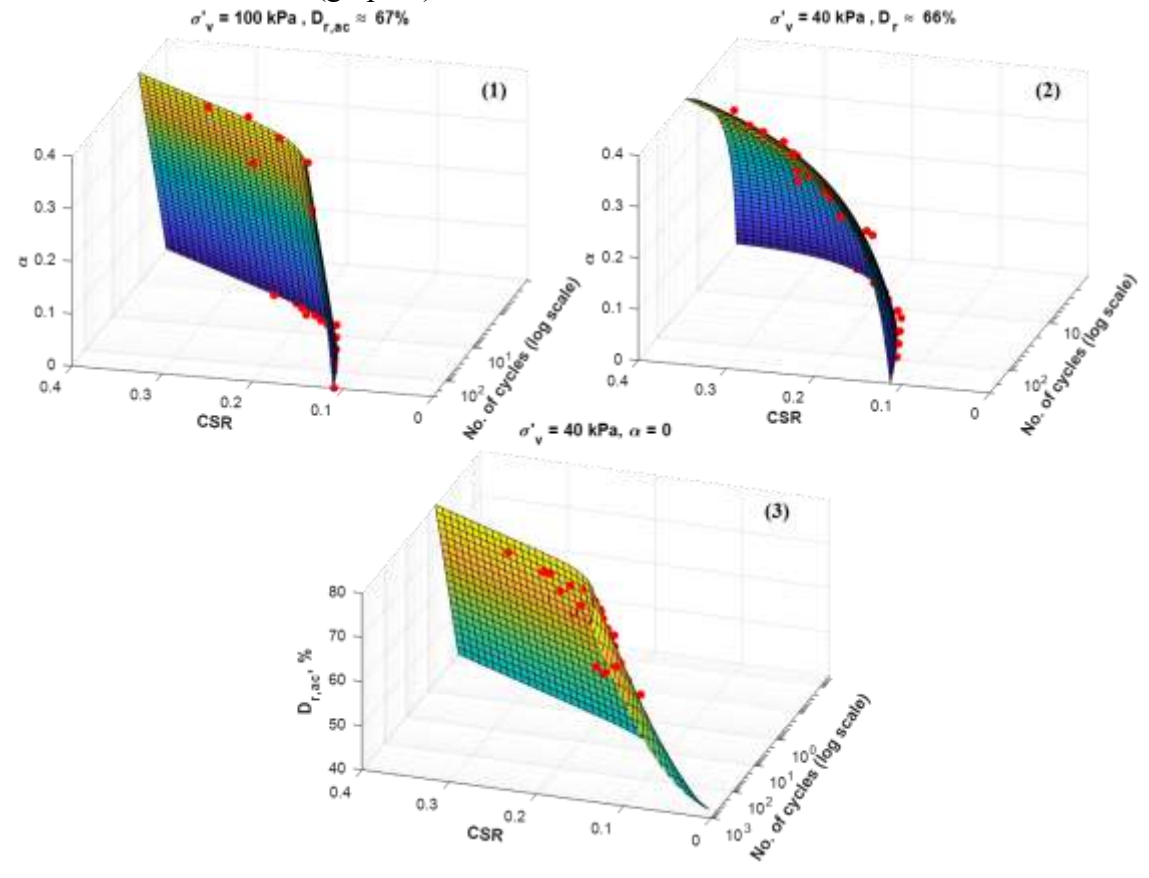


Figure 14: Surface plots of static shear stress ratio with cyclic stress ratio and number of cycles for $\sigma'_v = 100 \ kPa$ (1) and $\sigma'_v = 40 \ kPa$ (2), and surface plot of relative density with cyclic stress ratio and number of cycles for $\sigma'_v = 40 \ kPa$ (3).

The surface plots presented in Figure 14 were generated respectively using equations (1), (2), and (3) corresponding respectively to graphs (1), (2), and (3) and defined as follows:

$$Ncyc = 10^{a \times \exp(b \times \alpha + c \times CSR^2) + d \times CSR + f \times \alpha + g}$$
 (1)

560 where Ncyc is the number of cycles to reach 5% shear strain, CSR is the cyclic stress ratio, α is 561 the static shear stress ratio, and a, b, c, d, f, g are fitting parameters given by: a = 7.176, b =

562 1.717×10^{-1} , $c = -1.252 \times 10^{2}$, d = -6.811, f = 2.581, g = 1.682.

$$Ncyc = 10^{a_0 + \frac{a_1}{1 + e^{a_2(a_3 \times CSR + a_4 \times \alpha + a_5 \times CSR \times \alpha)}}}$$
 (2)

where Ncyc is the number of cycles to reach 7.5% shear strain, CSR is the cyclic stress ratio, α is 564

- 565 the static shear stress ratio, and a_0 , a_1 , a_2 , a_3 , a_4 , a_5 are fitting parameters given by: $a_0 =$
- -1.914×10^{-2} , $a_1 = 1.684 \times 10^1$, $a_2 = 5.956 \times 10^{-1}$, $a_3 = 2.586 \times 10^1$, $a_4 = 3.791$, $a_5 = 1.684 \times 10^1$ 566
- -4.817×10^{1} . 567

580

581

$$Ncyc = 10^{a \times \exp(b \times D_r + c \times CSR^2) + d \times CSR + f \times D_r + g}$$
 (3)

- 569 where Ncyc is the number of cycles to reach 7.5% shear strain, CSR is the cyclic stress ratio, $D_{r,ac}$
- is the relative density, and a, b, c, d, f, g are fitting parameters given by: $a = 7.247 \times 10^{-2}$, b =570
- 7.096×10^{-2} , $c = -1.431 \times 10^{2}$, d = -7.375, $f = 2.627 \times 10^{-2}$. 571
- 572 From equations (1), (2), and (3), it can be concluded that the number of cycles Ncyc to reach 5%
- 573 or 7.5% shear strain increases with increase in CSR, increase in static shear stress ratio α , or
- 574 increase in relative density $D_{r,ac}$. This agrees with previous conclusions stating that the cyclic
- 575 strength of Ottawa F65 sand increases with higher static shear stress and higher relative density.
- 576 The increase of Ncyc with α is more pronounced for low CSR values, and the increase of Ncyc
- 577 with decreased CSR is slightly more pronounced at higher values of α . Moreover, the increase of
- 578 Ncyc with $D_{r.ac}$ is more pronounced for low CSR values, and the increase of Ncyc with decreased
- 579 CSR is slightly more pronounced for higher values of $D_{r,ac}$.

3.3. Modeling of Soil Response using Artificial Neural Networks

3.3.1. Development of the Neural Networks model

- 582 The database of CDSS tests developed in this study (54 CDSS tests) and the CDSS tests conducted
- 583 by ElGhoraiby et al. [32] (11 CDSS tests) is used to develop an Artificial Neural Network (ANN)
- model trained to predict the cyclic strength of Ottawa F65 sand for a specified set of vertical 584
- 585 effective stresses, cyclic stress ratios, static shear stress ratios and relative densities after
- 586 consolidation. The ANN model relates an output variable represented by the number of cycles
- 587
- required to reach 2.5%, 5% or 7.5% shear strain to four input variables including soil relative density after consolidation $D_{r,ac}$ (55.2%, 66.2%, 71.2%, 75.5%), vertical confining stress σ'_{v} (40 588
- 589 kPa, 100 kPa), static shear stress ratio α (0, 0.25, 0.375, 0.4), and cyclic stress ratio CSR ranging
- 590 from 0.1 to 0.35. The logarithm of the number of cycles was used to limit variations in the output
- 591 data and improve the model predictive capability. The ANN model includes an input layer with
- 592 four neurons representing the four input variables, a hidden layer with four neurons, and an output
- 593 layer with one neuron representing the logarithm of the number of cycles required for Ottawa F65
- 594 sand to reach 2.5% 5%, or 7.5% shear strain noted Neve. The ANN model was designed by trial
- 595 and error considering the performance of the model during training, validation and testing. Figure
- 596 15 presents the architecture of the ANN model used.

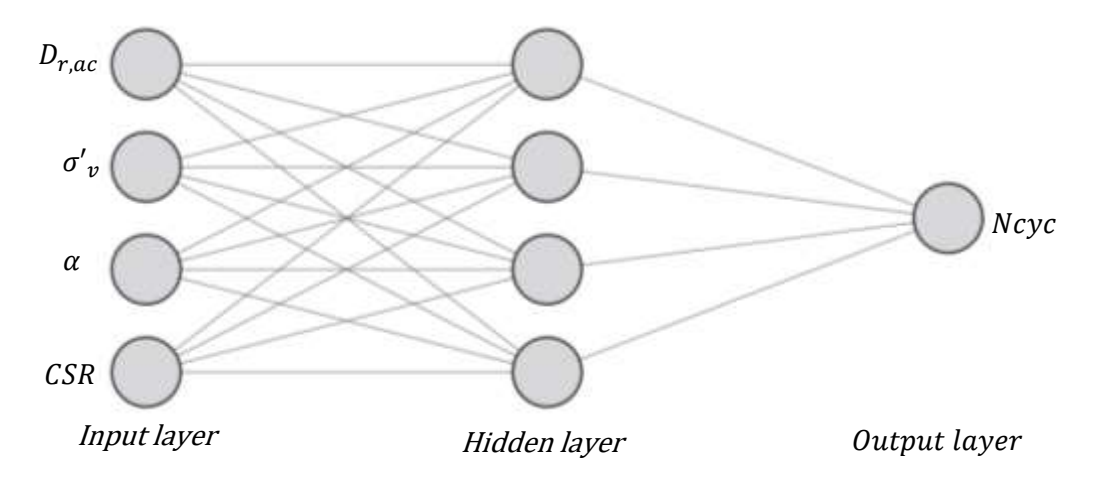


Figure 15: Architecture of the ANN model.

3.3.2. Training of the Neural Networks model

597

598

599

600

601

602

603

604

605

606

607

608

609

610

611

612613

614

The ANN model is trained using feed-forward and back propagation methods. A hyperbolic tangent function was used as the activation function for connections between the input layer and the hidden layer, and a rectified linear unit function was used as the activation function for connections between the hidden layer and the output layer. Since the output variable contains continuous real numbers, the mean squared error was used as loss function quantifying the total loss created by incorrect predictions. The ANN model was developed using the Neural Network Toolbox in Matlab [43]. First, the ANN model was trained to capture the number of cycles required to reach 7.5% double amplitude shear strain for CDSS tests conducted without static shear stress. For this purpose, a total of 43 CDSS tests were used including tests conducted at vertical stresses of 40 kPa and 100 kPa, relative densities of approximately 55%, 66%, 71% and 75%, and various cyclic stress ratios. The dataset of 43 CDSS tests do not include CDSS tests conducted with static shear stress. The model was trained on 72% of the training data base (31 CDSS tests), and 28% of the training dataset (12 CDSS tests) was reserved for validation and testing of the model. In a study by Gholamy et al. [44], it was reported that empirical studies have shown that the best results are obtained if 70% to 80% of the data is reserved for training and 20% to 30% of the data is reserved for testing. The study has provided a theoretical explanation of such observations from empirical studies.

Figure 16 presents the evolution of the mean squared error with epochs for the train, validation, and test batches. An epoch corresponds to training the neural network model with all the training data for one cycle including a forward pass and a backward pass. The best performance of the model was achieved at epoch 92 where the gradient decent was equal to 0.009.

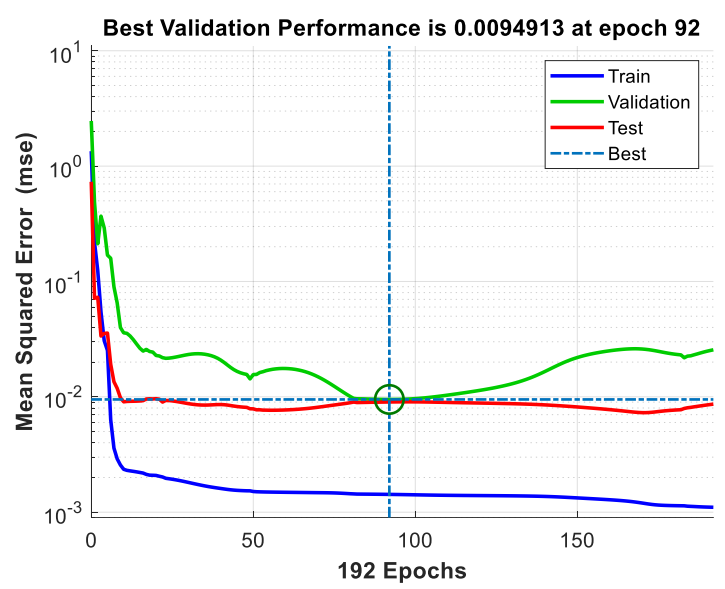


Figure 16: Performance of the ANN model in terms of mean squared error evolution.

Figure 17 presents results of the ANN model predictions on the training, validation and testing dataset of CDSS tests conducted at vertical effective stresses of 40 kPa and 100 kPa on specimens prepared at relative densities after consolidation of about 55.2%, 66.2%, 71.2% and 75.5%. It is shown that the ANN predictions are close to the experimental results and that the ANN model is sensitive to changes in overburden stress and relative density.

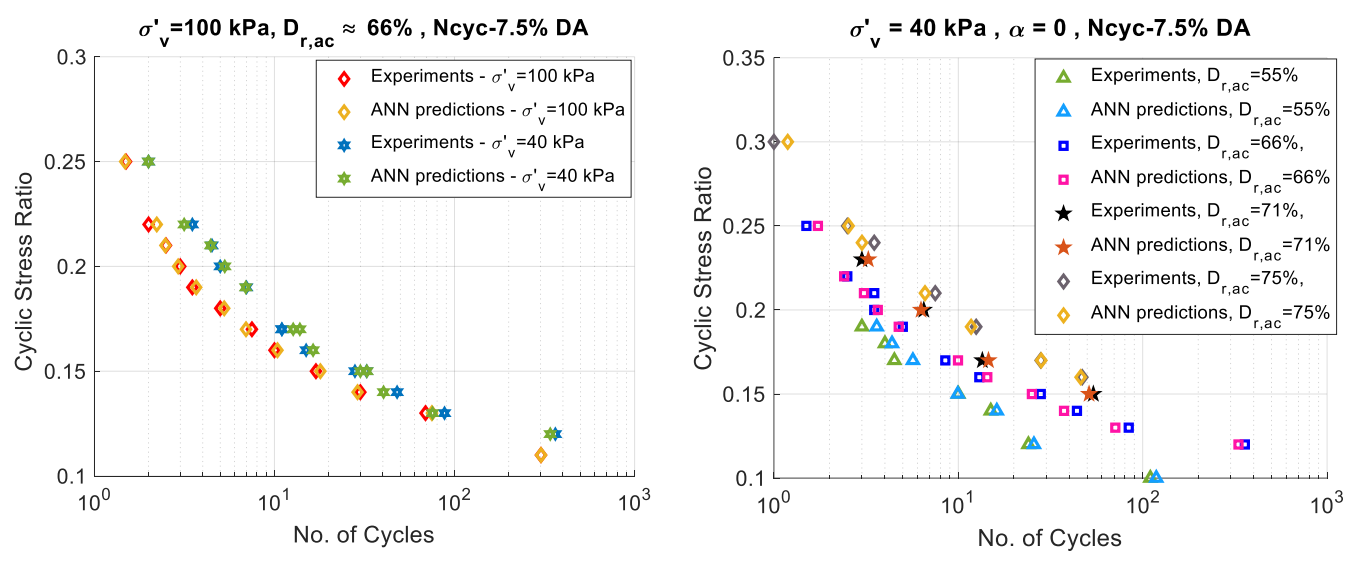


Figure 17: ANN model performance on the training dataset for $\sigma'_{v} = 40 \, kPa$, $100 \, kPa$, $D_{r,ac} \approx 66\%$, $\alpha = 0$ (left) and for $\sigma'_{v} = 40 \, kPa$, $D_{r,ac} \approx 55\%$, 66%, 71%, 75%, $\alpha = 0$ (right).

The training of the ANN model was then extended to include the effect of static shear stress. For this purpose, CDSS tests conducted with static initial shear stress at a vertical stress of 40 kPa were included in the training dataset. The ANN model was trained to capture the number of cycles required to reach 7.5% double amplitude shear strain. A total of 57 CDSS tests were used, which corresponds to the entire dataset except for CDSS tests conducted at a vertical stress of 100 kPa

and static shear stresses of 30 kPa and 40 kPa for which the shear strain did not reach 7.5% shear strain amplitude. The model was trained on 68% of the training data base (39 CDSS tests), and 32% of the training dataset (18 CDSS tests) was reserved for validation and testing of the model. Figure 18 (left) presents results of the ANN model predictions on the training, validation, and testing dataset of CDSS tests conducted at vertical effective stresses of 40 kPa with static shear stress ratios of 0, 0.25, and 0.375. It is shown that the ANN predictions are close to the experimental results and that the ANN model is sensitive to changes in static shear stress ratio.

To extend the model predictions beyond one level of shear strain, the ANN model was trained to predict the number of cycles required to reach 2.5% and 5%, in addition to 7.5% double amplitude shear strain developed earlier. The model was trained on 70% of the training data base (45 CDSS tests), and 30% of the training dataset (20 CDSS tests) was reserved for validation and testing of the model. Figure 18 (right) presents results of the ANN model predictions on the training, validation and testing dataset of CDSS tests conducted at vertical effective stresses of 100 kPa with static shear stress ratios of 0, 0.3, and 0.4. Again, the ANN model is sensitive to change in static shear stress ratio.

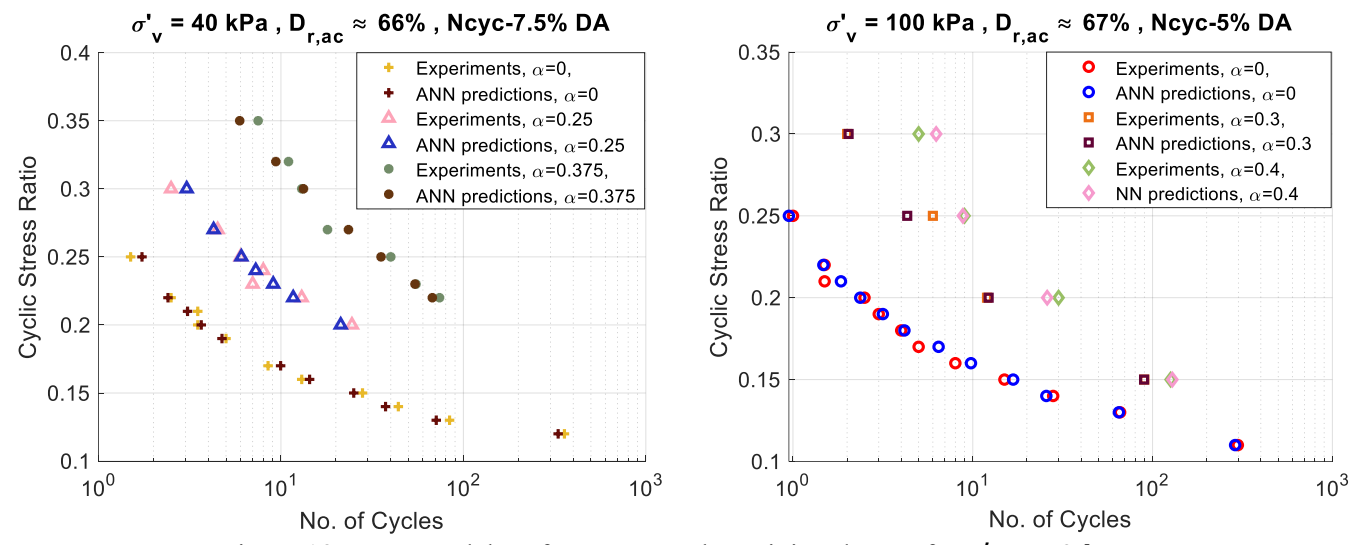


Figure 18: ANN model performance on the training dataset for $\sigma'_v = 40 \ kPa$, $D_{r,ac} \approx 66\%$, $\alpha = 0, 0.25, 0.375$ (left) and for $\sigma'_v = 100$ kPa, $D_{r,ac} \approx 67\%$, $\alpha = 0, 0.3, 0.4$ (right).

Figure 19 shows the experimental and ANN-predicted scatter plots of cyclic stress ratio variation with the number of cycles to reach 2.5%, 5% and 7.5% double amplitude shear strain for CDSS tests conducted at a vertical effective stress of 100 kPa with no static shear stress. The ANN model shows sensitivity to the achieved shear strain amplitude as more cycles are generally required in the ANN predictions to reach a higher shear strain.

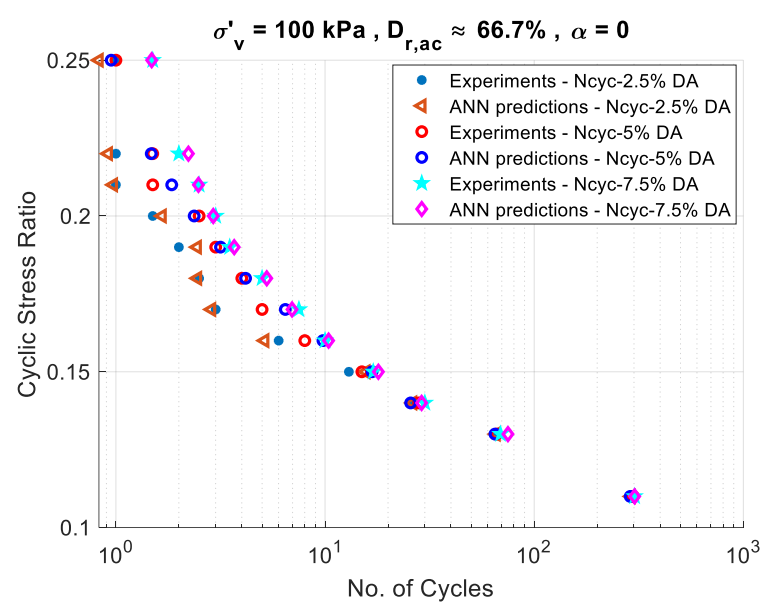


Figure 19: ANN model performance on the training dataset for $\sigma'_v = 100 \ kPa$, $D_{r,ac} \approx 67\%$, Ncyc - 2.5%, 5%, 7.5% DA.

Figure 20 presents a plot of ANN-predicted versus measured number of cycles required to reach 7.5% shear strain. The plot pictures the overall performance of the ANN model during training, validation and testing.

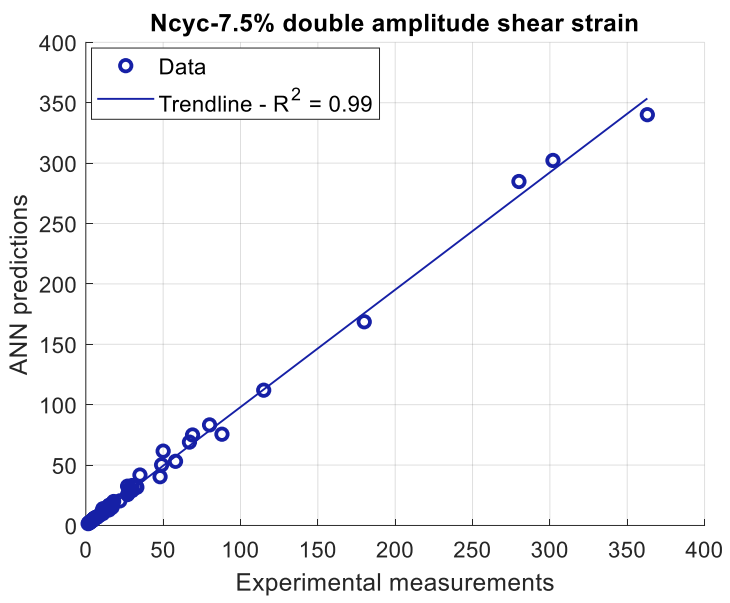


Figure 20: ANN-predicted versus measured number of cycles required to reach 7.5% shear strain.

3.3.3. Validation of the Neural Networks model using blind predictions

649

650

651 652

653

The ANN model was further assessed and validated using blind predictions of new CDSS tests (to be conducted) at a relative density after consoldation of 60% under a vertical effective stress of 70 kPa. The predictions considered cyclic stress ratios (*CSRs*) of 0.1, 0.15, 0.20, 0.25, and 0.30 and zero static shear stress prior to cyclic shearing. Figure 21 presents the ANN blind predictions of

the number of cycles (*Ncyc*) required to reach 2.5%, 5% and 7.5% shear strain for each cyclic stress ratio, as well as the corresponding liquefaction strength curves.

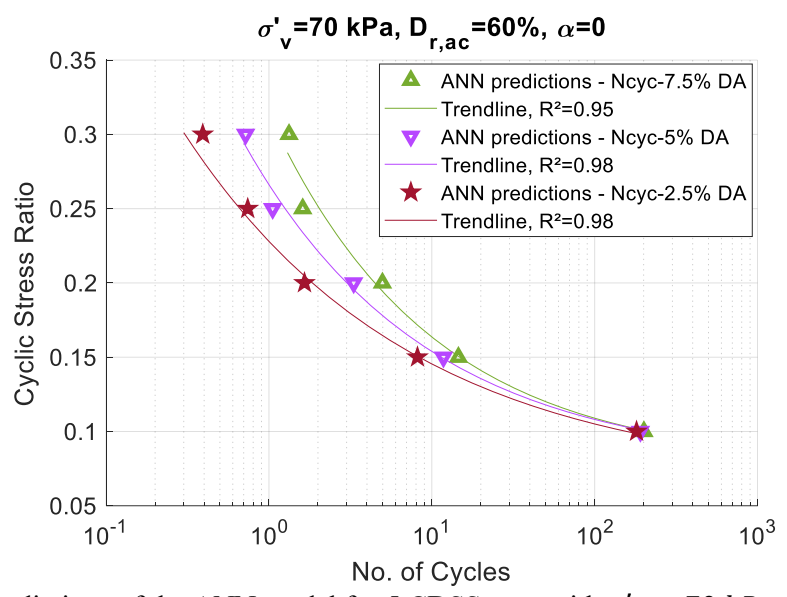


Figure 21: Blind predictions of the ANN model for 5 CDSS tests with $\sigma'_v = 70 \ kPa$ and $D_{r,ac} = 60\%$.

Afterwards, five CDSS tests were conducted on Ottawa F65 specimens prepared under similar conditions as those considered in the blind predictions. Table 12 summarizes key information about the five cyclic direct simple shear tests conducted to assess and validate the ANN model performance. The Table includes values of the dry density before consolidation (ρ_d), void ratio after consolidation (e_{ac}), relative density after consolidation ($D_{r,ac}$), cyclic stress ratio (CSR), and the number of cycles required to reach 1.5%, 2.5%, 5% and 7.5% double amplitude shear strain (Ncyc - 1.5%, Ncyc - 2.5%, Ncyc - 5%, Ncyc - 7.5%). Figure 22 presents an example of test results in terms of stress-strain response and stress path for a constant volume cyclic direct simple shear test conducted at $D_{r,ac} = 66.43\%$, $\sigma'_v = 70$ kPa, $\sigma'_v = 70$ kPa, $\sigma'_v = 70$ kPa, $\sigma'_v = 70$ kPa, $\sigma'_v = 70$ kPa.

Test No.	$\rho_d(kg/m^3)$	e _{ac}	D _{r,ac} (%)	CSR	<i>Ncyc</i> -1.5%	<i>Ncyc</i> - 2.5%	<i>Ncyc</i> – 5%	<i>Ncyc</i> - 7.5%
1	1621	0.621	58.9	0.1	182	188	197	208
2	1624	0.618	59.9	0.15	7	9	11.5	14
3	1621	0.615	61.2	0.2	1	2	5	6.5
4	1617	0.617	60.4	0.25	1	1	1.5	2.5
5	1616	0.622	58.7	0.3	0.5	0.5	1	1.5
Average	1620	0.619	59.8					
COV (0/.)	0.2	0.4	1.6	1				

Table 12: Summary of constant volume cyclic direct simple shear tests with $\sigma'_v = 70$ kPa and $D_{r,ac} \approx 60\%$.

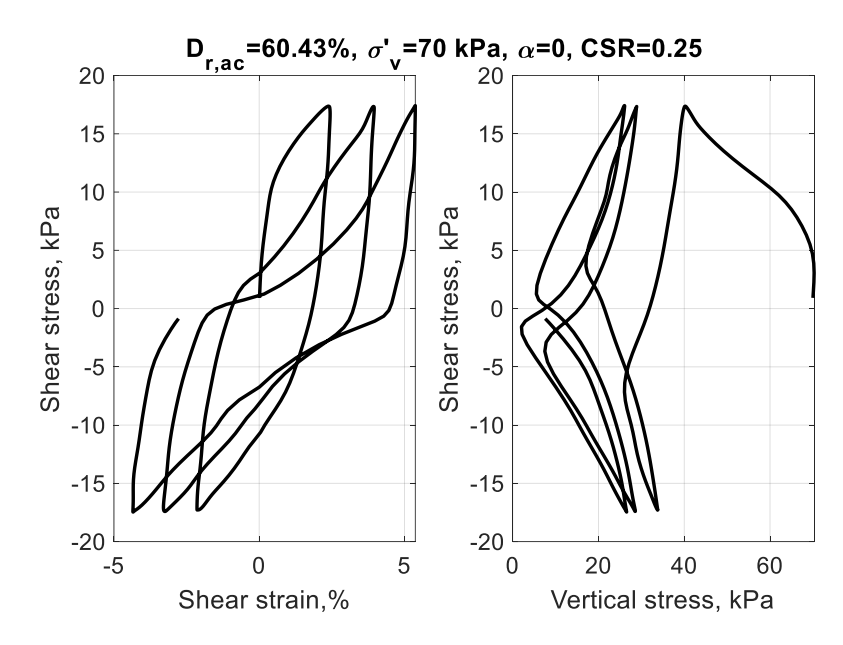


Figure 22: An example of the stress-strain response and stress path of the constant volume CDSS tests used for validation of the ANN model using blind predictions.

Figure 23 presents the CDSS test results against the ANN model blind predictions presented in scatter plots of the cyclic stress ratio variation with the number of cycles required to reach 7.5%, 5%, and 2.5% shear strain, and the corresponding liquefaction strength curves (Figure 23 (a), Figure 23 (b), and Figure 23 (c), respectively). By considering the surface areas underneath experimental versus ANN-predicted liquefaction strength curves, the respective errors of the ANN predictions for 7.5%, 5% and 2.5% double amplitude shear strain were estimated at 0.51%, 1.33%, and 0.91%. It is also noted that the ANN predictions are considered conservative since the ANN model predicts smaller number of cycles to reach liquefaction under a given cyclic stress ratio.

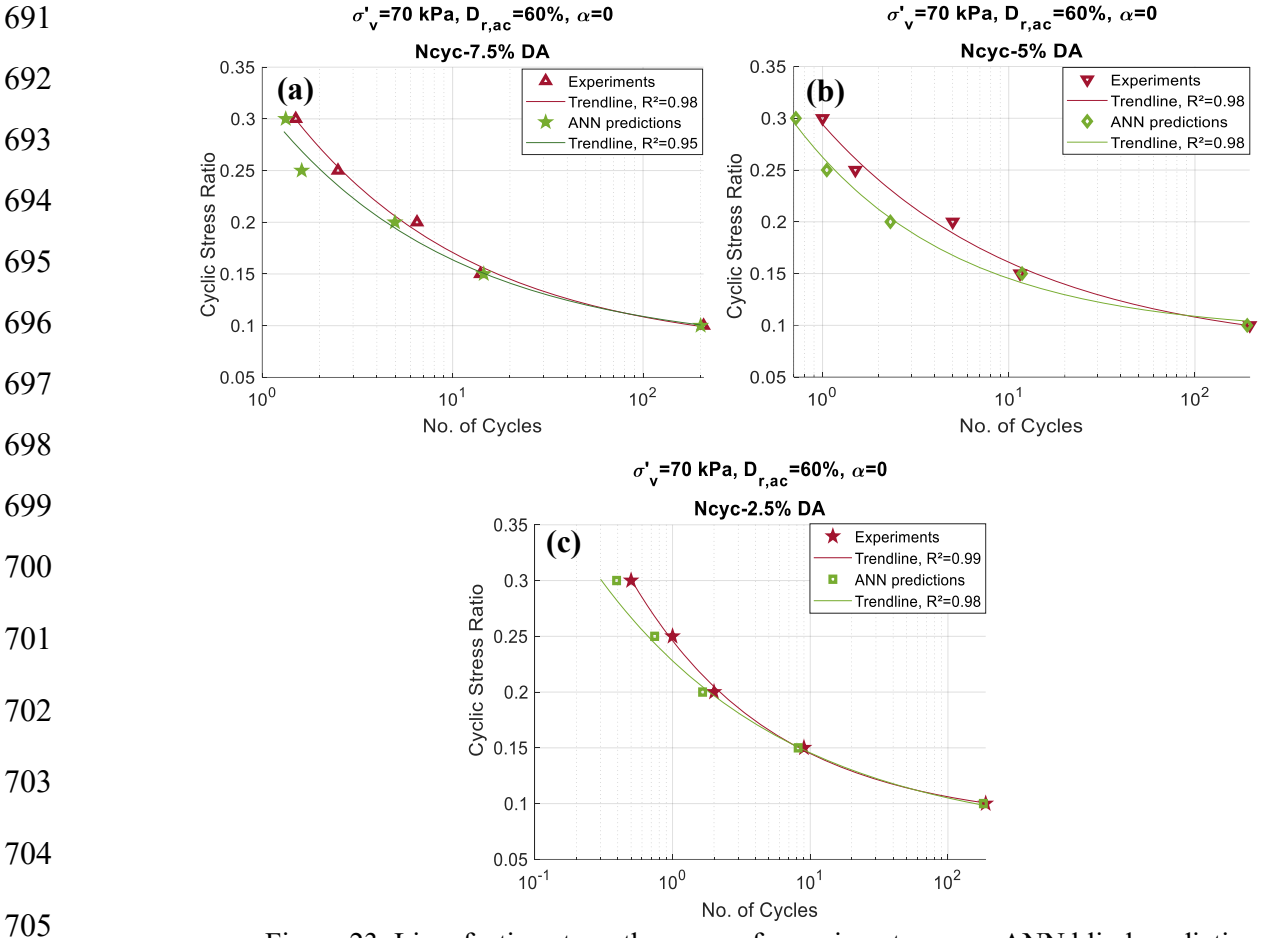


Figure 23: Liquefaction strength curves of experiments versus ANN blind predictions, Ncyc - 7.5% (a), Ncyc - 5% (b), Ncyc - 2.5% (c).

In order to verify whether the error of ANN predictions is related to variation of relative density around 60% in the five CDSS tests conducted (coefficient of variation of 1.6%), additional predictions of the ANN model were performed for a vertical effective stress of 70 kPa with relative densities of 59% and 61% in addition to the previous predictions with a relative density of 60% as shown in Figure 24. It is noted from Figure 24 that the ANN model is sensitive to the slight change in the soil relative density, but the small variation of the achieved relative densities in the experiments does not justify the observed error in ANN predictions relative to the experiments for the relative density of 60%.

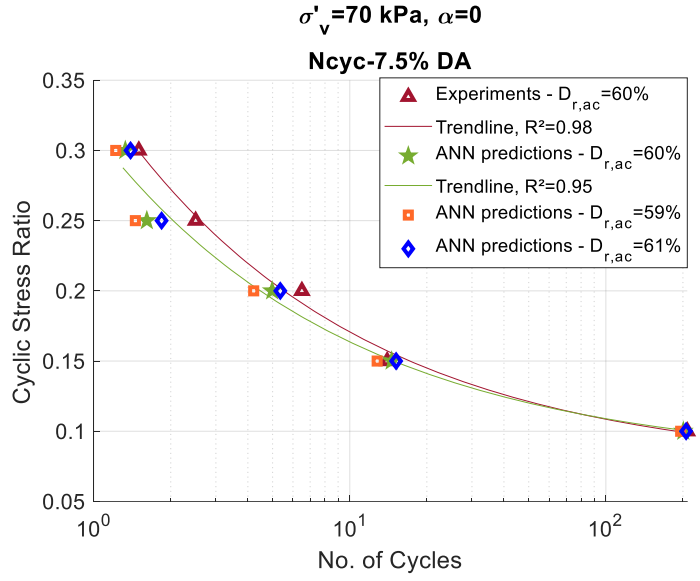


Figure 24: Liquefaction strength curves of experiments versus ANN blind predictions, $D_{r,ac} = 59\%, 60\%, 61\%$.

Overall, the ANN model predictions were sensitive to increased relative density, increased static shear stress ratio, and increased cyclic stress ratio during training, validation, and testing (Figures 17-19). The number of cycles predicted by the ANN model increased with higher relative density and higher static initial shear stress ratio and decreased with higher cyclic stress ratio. During the validation of the model using blind predictions, the results have also shown sensitivity to change in cyclic stress ratio and relative density (Figure 24). The ANN predictions of cyclic strength were conservative as the model generally predicted a smaller number of cycles to reach 2.5%, 5%, or 7.5% double amplitude shear strain compared to the experimental number of cycles (Figure 23). The error of the ANN model predictions relative to measurements of the number of cycles were relatively small by considering surface areas underneath the ANN-predicted versus experimental liquefaction strength curves (error less than 2% on the surface area). Therefore, it can be concluded that the ANN model has shown capability of reasonable predictions of the cyclic strength of Ottawa F65 sand as well as sensitivity to changes in vertical stress, soil density, static shear stress ratio, and cyclic stress ratio.

4. Summary and concluding remarks

This study investigated the stress-strain response and liquefaction strength of Ottawa F65 sand through multiple series of stress-controlled constant volume cyclic direct simple shear (CDSS) tests. Specimens were prepared at four target relative densities ranging from 55% to 75% using a dry pluviation procedure, anisotropically consolidated at vertical stresses of 40 kPa and 100 kPa, subjected to static initial shear stress ratios ranging from 0 to 0.4, and then subjected to cyclic shearing. The collected dataset of constant volume CDSS tests was used to train an Artificial Neural Networks model with the objective to predict the cyclic strength of Ottawa F65 sand for densities and loading conditions that are not available in the experimental dataset. Key finding of the study are as follows:

1) An approximately 19% increase in cyclic strength (CRR corresponding to 15 uniform cycles) was observed when the soil relative density was increased by 10%.

- 2) The shear wave velocities measured before subjecting the soil specimens to cyclic loading showed an increasing trend with increased soil density. This confirms the increase of shear wave velocity and shear modulus with increased soil density.
- 3) CDSS tests on specimens prepared at a target relative density of 66% and subjected to vertical consolidation stresses of 40 kPa and 100 kPa have demonstrated that cyclic strength of Ottawa F65 sand decreases with increased vertical stress for this relative density. The corresponding liquefaction strength curves showed a good agreement with the CDSS tests conducted by ElGhoraiby et al. [32] for similar relative density and vertical stresses, and smaller values of cyclic stress ratio.
- 4) CDSS tests conducted by considering a static initial shear stress prior to cyclic shearing have demonstrated that cyclic strength increases with increased static initial shear stress for a target density of 66%. These experiments included tests subjected to a vertical consolidation stress of 40 kPa and then subjected to static initial shear stress ratios ranging from 0 to 0.375, and tests subjected to a vertical consolidation stress of 100 kPa and then subjected to static initial shear stress ratios ranging from 0 to 0.4.
- 5) The empirical correction factor K_{α} to account for the effect of static shear stress ratio on the liquefaction strength of sandy soils developed by Idriss and Boulanger [9] provided larger values compared to the ratio of the CRR values $(CRR_{\alpha}/CRR_{\alpha=0})$ obtained from the tests conducted in this study.
- 6) The empirical correction factor K_{σ} , proposed by Idriss and Boulanger [9] to account for the increase in cyclic strength due to the decrease in confining stress, provided a slightly lower value compared to the ratio of CRR values CRR_{40}/CRR_{100} obtained from the CDSS tests (CRR_{40} and CRR_{100} respectively correspond to the CRR at 15 uniform cycles for tests conducted under vertical stresses of 40 kPa and 100 kPa).
- 7) Surface plots were used to approximate the variation of cyclic strength (Ncyc 7.5% for vertical stress of 40 kPa and Ncyc 5% for vertical stress of 100 kPa) with static initial shear stress ratio α and cyclic stress ratio CSR. The variation suggested that the increase of Ncyc with α is more pronounced for low CSR values, and the increase of Ncyc with decreased CSR is slightly more pronounced for higher values of α .
- 8) A surface plot was used to approximate the variation of cyclic strength (Ncyc 7.5%) with relative density $D_{r,ac}$ and cyclic stress ratio CSR. The variation suggested that the increase of Ncyc with $D_{r,ac}$ is more pronounced for low CSR values, and the increase of Ncyc with decreased CSR is slightly more pronounced for higher values of $D_{r,ac}$.
- 9) The Artificial Neural Networks (ANN) model trained on the collected dataset of constant volume CDSS tests has shown capability of reasonable predictions of cyclic strength Ottawa F65 sand as well as sensitivity to changes in vertical stress, soil density, static shear stress, and cyclic stress ratio. The ANN model can potentially be used in predicting cyclic strength of Ottawa F65 sand under new loading conditions and soil density that are not available in the experimental database.

783 Acknowledgement

- 784 LEAP-2020 and LEAP-2022 projects have been funded by the National Science Foundation grants
- 785 CMMI-1635524 to the George Washington University. This support is gratefully acknowledged.

786 Author contributions

- 787 **Sarra Lbibb**: Data curation, Investigation, Methodology, Formal analysis, Software, Validation,
- 788 Visualization, Writing original draft.
- 789 **Majid T. Manzari**: Supervision, Project administration, Funding acquisition, Conceptualization,
- 790 Investigation, Methodology, Formal analysis, Validation, Visualization, Writing review &
- 791 editing.

792 **References**

- 793 [1] Seed, H.B., Idriss, I.M. Ground Motions and Soil Liquefaction during Earthquakes. Earthquake 794 Engineering Research Institute Monograph, Oakland, 1982.
- 795 [2] Finn, W., Vaid, Y., Bhatia, S. K. Constant Volume Cyclic Simple Shear Testing: Second
 796 International Conference on Microzonation for Safer Construction: Research and Applications
 797 1978; 839 851.
- 798 [3] Wijewickreme, D., Sriskandakumar, S., Byrne, P. Cyclic loading response of loose air-799 pluviated Fraser River sand for validation of numerical models simulating centrifuge tests. 800 Canadian Geotechnical Journal 2005, 42(2), 550-561.
- 801 [4] Da Fonseca, A. V., Soares, M., Fourie, A. B. Cyclic DSS tests for the evaluation of stress densification effects in liquefaction assessment. Soil Dynamics and Earthquake Engineering 2005, 75, 98-111.
- [5] Seed, H. B. and Lee, K. L. Liquefaction of saturated sands during cyclic loading. Journal of the Soil Mechanics and Foundations Division 1966, 92(6), 105-134.
- 806 [6] Wai, D., Manmatharajan, M. V. and Ghafghazi, M. Effects of Imperfect Simple Shear Test
 807 Boundary Conditions on Monotonic and Cyclic Measurements in Sand. Journal of
 808 Geotechnical and Geoenvironmental Engineering, 148(1) 2022.
 809 https://doi.org/10.1061/(ASCE)GT.1943-5606.0002682.
- [7] Castro, G., & Poulos, S. J. Factors affecting liquefaction and cyclic mobility. Journal of the Geotechnical Engineering Division 1977, *103*(6), 501-516.
- 812 [8] Ishihara, K. Soil behaviour in earthquake geotechnics. Oxford Engineering Science Series 1996, 46.
- [9] Idriss, I.M. and Boulanger, R.W. Soil Liquefaction during Earthquake. EERI Publication, Monograph MNO-12, Earthquake Engineering Research Institute, Oakland, 2008.
- [10] Seed, H. B. Earthquake resistant design of earth dams. Proc., Symposium on Seismic Design of Embankments and Caverns, Pennsylvania, 1983, ASCE, N.Y., 41-64.

- 818 [11] Boulanger, R. W. Relating K_{α} to relative state parameter index. Journal of Geotechnical and Geoenvironmental Engineering 2003, 129(8), 770-773.
- [12] Park, S. S., Nong, Z. Z., & Lee, D. E. Effect of vertical effective and initial static shear stresses on the liquefaction resistance of sands in cyclic direct simple shear tests. Soils and Foundations 2020, 60(6), 1588-1607. https://doi.org/10.1016/j.sandf.2020.09.007.
- 823 [13] Boulanger, R. W. and Idriss, I. M. Evaluating the potential for liquefaction or cyclic failure 824 of silts and clays (p. 131), 2004. Davis, California: Center for Geotechnical Modeling.
- 825 [14] Peacock, W. H. and Seed, H. B. Sand liquefaction under cyclic loading simple shear conditions. Journal of the Soil Mechanics and Foundations Division 1968, *94*(3), 689-708.
- [15] Yoshimi, Y. and Oh-oka, H. Influence of degree of shear stress reversal on the liquefaction potential of saturated sand. Soils and foundations 1975, *15*(3), 27-40.
- [16] Wong, R. T., Seed, H. B. and Chan, C. K. Cyclic loading liquefaction of gravelly soils. Journal of the Geotechnical Engineering Division 1975, *101*(6), 571-583.
- [17] Tatsuoka, F., Toki, S., Miura, S., Kato, H., Okamoto, M., Yamada, S. I., ... and Tanizawa, F. Some factors affecting cyclic undrained triaxial strength of sand. Soils and foundations 1986, 26(3), 99-116.
- [18] Lee, K. L. and Fitton, J. A. Factors affecting the cyclic loading strength of soil 1969 (pp. 71-95). ASTM International.
- [19] Feng, T. G. and Zhang, L. M. Experimental study on effect of vibration frequency on dynamic behaviors of saturated loose sands. Journal of Water Resources and Architectural Engineering 2013, 11(3), 11-14.
- [20] Ying, G. U. O., and Lin, H. E. The influences of the vibration frequencies on liquefaction strength of saturated sands. Journal of Disaster Prevention and Mitigation Engineering 2009.
- [21] Cappellaro, C., Cubrinovski, M., Bray, J. D., Chiaro, G., Riemer, M. F., Stringer, M. E. Liquefaction resistance of Christchurch sandy soils from direct simple shear tests. Soil Dynamics and Earthquake Engineering 2021, 141, 106489. https://doi.org/10.1016/j.soildyn.2020.106489.
- 845 [22] Manzari, M.T., Kutter, B. L., Zeghal, M., ... and Zhou, YG. LEAP projects: Concept and 846 challenge. Proceedings of the 4th International Conference on Geotechnical Engineering 847 for Disaster Mitigation and Rehabilitation, Kyoto, 2014.
- [23] Manzari, M., ElGhoraiby, M. E., Kutter, B. L., ..., and Ziotopoulou, K. Liquefaction analysis and experiment projects (LEAP): Summary of observations from the planning phase. International Journal of Soil Dynamics and Earthquake Engineering 2017, https://doi.org/10.1016/j.soildyn.2017.05.015.
- 852 [24] Manzari, M. T., ElGhoraiby, M.A., Kutter, B. L., ..., Escoffier, S. LEAP-2017 Simulation 853 Exercise: Calibration of Constitutive Models and Simulation of the Element Test. In: 854 Kutter, B., Manzari, M., Zeghal, M. (eds) Model Tests and Numerical Simulations of

- Liquefaction and Lateral Spreading 2020. Springer, Cham. https://doi.org/10.1007/978-3-856
 030-22818-7 9.
- 857 [25] Kutter, B. L., Carey, T. J., Hashimoto, ..., Manzari, M. T. LEAP-GWU-2015 experiment 858 specifications, results, and comparisons. Soil Dynamics and Earthquake Engineering 2018, 859 113, 616-628.
- [26] Kutter BL, Carey TJ, Stone N, Zheng BL, Gavras A, Manzari M.T., et al. LEAP-UCD2017
 Comparison of Centrifuge Test Results. Cham: Springer International Publishing; 2020.
 https://doi.org/10.1007/978-3-030-22818-7.
- [27] Ueda, K., Vargas, R., Uemura, K. LEAP-Asia-2018: stress-strain response of Ottawa sand in
 cyclic torsional shear tests. DesignSafe-CI. Alexandria, VA: National Science Foundation,
 2018.
- 866 [28] Wichtmann, T., Triantafyllidis, T. Behaviour of granular soils under environmentally induced 867 cyclic loads. In Mechanical behaviour of soils under environmentally induced cyclic 868 loads (pp. 1-136). Springer, Vienna, 2012.
- 869 [29] Vasko, A. An investigation into the behavior of Ottawa sand through monotonic and cyclic shear tests. The George Washington University, 2015.
- 871 [30] Bastidas, A. M. P. Ottawa F65 sand characterization. University of California, Davis, 2016.
- [31] Carey, T.J., Stone, N. and Kutter, B.L. Grain Size Analysis and Maximum and Minimum Dry
 Density Testing of Ottawa F65 Sand for LEAP-UCD-2017. In: Kutter, B., Manzari, M.,
 Zeghal, M. (eds) Model Tests and Numerical Simulations of Liquefaction and Lateral
 Spreading 2020. Springer, Cham. https://doi.org/10.1007/978-3-030-22818-7 2.
- 876 [32] ElGhoraiby, M. A., Park, H. and Manzari, M. T. Stress-strain behavior and liquefaction 877 strength characteristics of Ottawa F65 sand. Soil Dynamics and Earthquake Engineering 878 2020, 138, 106292.
- [33] Vargas, R. R., Ueda, K., Uemura, K. Influence of the relative density and K0 effects in the
 cyclic response of Ottawa F65 sand-cyclic Torsional Hollow-Cylinder shear tests for LEAP ASIA-2019. Soil Dynamics and Earthquake Engineering 2020, 133, 106111.
- 882 [34] Goh, A. T. Seismic liquefaction potential assessed by neural networks. Journal of Geotechnical engineering 1994, 120(9), 1467-1480.
- 884 [35] Goh, A. T. Neural-network modeling of CPT seismic liquefaction data. Journal of Geotechnical engineering 1996, 122(1), 70-73.
- 886 [36] Ali, H. E. and Najjar, Y. M. Neuronet-based approach for assessing liquefaction potential of soils. Transportation Research Record 1998, 1633(1), 3-8.
- [37] Juang, C. H., Yuan, H., Lee, D. H., Lin, P. S. Simplified cone penetration test-based method for evaluating liquefaction resistance of soils. Journal of geotechnical and geoenvironmental engineering 2003, 129(1), 66-80.

- 891 [38] Young-Su, K., Byung-Tak, K. Use of artificial neural networks in the prediction of liquefaction resistance of sands. Journal of Geotechnical and Geoenvironmental Engineering 2006, 132(11), 1502-1504.
- 894 [39] Geocomp Corporation. Direct Simple Shear Software, ShearTrac-II DSS; Geocomp Corporation 2018: New York, NY, USA, 2018.
- 896 [40] www.bitbucket.org
- 897 [41] Whitley, D. A genetic algorithm tutorial. Statistics and computing 1994, 4(2), 65-85.
- 898 [42] Joshi, S., Singh, D., Kaur, M., Lee, H. N. Comprehensive Review of Orthogonal Regression 899 and its Applications in Different Domains. Archives of Computational Methods in 890 Engineering 2022, 1-21.
- 901 [43] Beale, M. H., Hagan, M. T. and Demuth, H. B. Neural network toolbox. User's Guide, MathWorks, 2010 2, 77-81.
- 903 [44] Gholamy, A., Kreinovich, V., Kosheleva, O. Why 70/30 or 80/20 relation between training and testing sets: a pedagogical explanation, 2018.